1   Pyrimidine sufficiency is required for Sae two-component system signaling in

2   *Staphylococcus aureus*

3

4   Dennis A. DiMaggio, Jr., Won-Sik Yeo, and Shaun R. Brinsmade

5   Department of Biology, Georgetown University, Washington, DC USA

6

7

8

9   Running Title: Pyrimidines promote Sae activity in *S. aureus*

10

11

12

13

14

15

16

17

18

19   Corresponding author: Shaun Brinsmade (shaun.brinsmade@georgetown.edu)

20

21

22   Key words: MRSA, *Staphylococcus aureus*, SaeRS, virulence, membrane, free fatty

23   acids, Pyrimidine metabolism, two-component regulatory systems, virulence regulation,

24   pyrimidine, metabolism

Abstract

Nucleotide metabolism in pathogens is essential for their virulence, supporting growth, survival, and immune evasion during infection. Virulence in *Staphylococcus aureus* is driven by the production of virulence factors that facilitate nutrient acquisition and promote immune evasion and subversion. One key virulence regulatory system is the Sae two-component system (TCS), which upregulates the production of various virulence factors. The sensor histidine kinase SaeS, a member of the intramembrane family of histidine kinases (IM-HKs), lacks a signal-binding domain, leaving the mechanisms by which these HKs sense signals and regulate gene expression unclear. We report that de novo pyrimidine biosynthesis is essential for maintaining Sae activity. Disruption of genes involved in pyrimidine biosynthesis reduces Sae-dependent promoter activity under pyrimidine-limited conditions. Phos-tag electrophoresis confirmed that pyrimidine limitation impacts SaeS kinase activity. The effect of pyrimidine limitation on SaeS was abrogated in a strain producing only the catalytic domain, suggesting that pyrimidines regulate SaeS activity at the membrane. Additionally, defective pyrimidine biosynthesis caused membrane defects and increased incorporation of free fatty acids into the membrane. Further, providing an extracellular sink for free fatty acids restored Sae activity in these mutants. Our study highlights the interplay between nucleotide metabolism and membrane integrity in regulating virulence factor expression through signal transduction systems in pathogens.

Importance

Virulence is often correlated with nutrient depletion, but our understanding of this coordination is incomplete. In *S. aureus*, the Sae two-component system (Sae TCS) is a major regulator of virulence factor production and secretion, but as the sensor histidine kinase SaeS lacks an obvious domain to perceive its inducing signal, basic questions surrounding how the kinase is triggered persist. This study aims to investigate the mechanism by which pyrimidines act to promote the activity of the SaeS kinase in *S. aureus* and further expands on the importance of the roles of pyrimidines in regulating envelope biogenesis. Understanding this intersection between nucleotide metabolism and virulence regulation opens up the possibility for the development of targeted anti-virulence strategies against *S. aureus* infections.

58 **Introduction**

59   *Staphylococcus aureus* is a Gram-positive, opportunistic human pathogen that

60   transiently colonizes the skin and anterior nares of approximately 30% of the human

61   population, with 20% being persistently colonized (1-3). Further, those that are stably

62   colonized are at a higher risk for developing an infection (4). *S. aureus* clinical

63   manifestations can initially present as mild to severe skin and soft tissue infections (5,

64   6). If left untreated, these infections can lead to more devastating invasive infections

65   such as infective endocarditis, osteomyelitis, and sepsis (7, 8). *S. aureus* has emerged

66   as one of the most devastating pathogens in healthcare. Although nosocomial infections

67   of *S. aureus* are a constant threat in healthcare settings, just as concerning are

68   infections caused by isolates circulating through the broader community (9). The

69   relatively recent increase in community acquired infections has been attributed in part to

70   metabolic adaptation and antimicrobial resistance. This has led to an uptick in the

71   number of *S. aureus* related deaths over the past decade, leading to a tremendous

72   financial burden on the US healthcare system, costing up to nearly $3 billion in annual

73   hospitalization costs (9, 10).

74

75   The survival and success of *S. aureus* as a pathogen fundamentally depends on its

76   ability to align its physiology to the host environment. It does so by coordinating central

77   metabolic processes with the production of virulence factors that serve to enhance

78   colonization while facilitating evasion from the host immune response. The combined

79   action of central metabolism and virulence factor production contribute to the fitness of

80   the bacterium, which is described by the capacity of the bacterium to adapt, replicate,

81   and persist within the host environment. One of the central metabolic pathways that has

82   emerged as a critical determinant of both bacterial fitness and virulence regulation is the

83   *de novo* pyrimidine biosynthetic pathway (9, 11), which provides essential precursors for

84   DNA and RNA synthesis, cell wall components, and various cellular cofactors (12). *De*

85   *novo* pyrimidine biosynthesis is a highly conserved metabolic process from microbes to

86   animals alike. Like in other organisms, *S. aureus* pyrimidine synthesis begins with the

87   synthesis of *N*-carbamoyl-*L*-aspartate. This first committed step is catalyzed by

88   aspartate transcarbamoylase (PyrB) and utilizes carbamoyl-phosphate, a common

89   metabolite in pyrimidine and nitrogen metabolism. Successive transformations by

90   dihydroorotase (PyrC), dihydroorotate dehydrogenase (PyrD), orotate

91   phosphoribosyltransferase (PyrE), and uridine monophosphate synthase (PyrF) result in

92   the formation of UMP (**Fig. 1A**) (13, 14). UMP can be further processed and converted

93   into the different pyrimidine nucleosides (uridine, cytidine, and thymidine) and

94   nucleobases (uracil, cytosine, and thymine) required for basic cellular processes (**Fig.**

95   **1A**) (13-16). The process of synthesizing pyrimidines *de novo* is regulated by the

96   pyrimidine biosynthesis regulator, PyrR (17). PyrR is predicted to be a bifunctional

97   protein that acts predominantly as a uridine-dependent transcriptional regulator on

98   expression of the pyrimidine biosynthetic gene cluster, but also acts as a uracil

99   phosphoribosyltransferase (UPRTase) (17-20). PyrR regulation occurs in a PRPP- and

100   UMP-dependent fashion. When intracellular levels of UMP are sufficient, PyrR binds to

101   UMP, which enhances PyrR-mRNA binding and promotes transcriptional attenuation of

102   the pyrimidine biosynthetic gene cluster (9, 19). Further, when UMP is low and PyrR

103   binds PRPP, there is a drop in the binding affinity of PyrR for its mRNA targets and

104   PyrR acts as a UPRTase to increase intracellular UMP levels. This pathway must be

105   properly regulated in *S. aureus* as pyrimidine metabolism is correlated with significant

106   impacts the overall fitness and virulence potential of the bacterium (9, 11, 21). Although

107   others have shown this correlation both *in vitro* and *in vivo*, the mechanism behind

108   pyrimidine-mediated regulation of virulence remains unclear.

109

110   Production of virulence factors may incur a fitness cost. This may explain in part the fact

111   that the expression and production of virulence factors is tightly controlled by a network

112   of regulatory systems, including transcriptional regulators, two-component systems, and

113   small regulatory RNAs (22-24). These systems enable *S. aureus* to occupy different

114   niches by sensing and responding to the various environmental conditions in a

115   coordinated manner and producing precisely the factors required for survival.

116   Understanding the mechanisms behind virulence factor regulation may provide novel

117   therapeutic targets for treating staphylococcal infections. A growing body of research

118   suggest so-called anti-virulence strategies offer an opportunity to mitigate the damage

119   *S. aureus* can cause by lowering or blocking the ability of the cells to produce virulence

120   factors (25-27).

121

122   One major regulator of *S. aureus* virulence is the SaeRS two-component system (TCS).

123   This TCS is responsible for regulating over 20 different secreted and surface-associated

124   virulence factors that facilitate nutrient acquisition and assist in evading and subverting

125   the immune response during infection (28). The *sae* (*S. aureus* exoprotein expression)

126   locus was discovered in 1994 by Giraudo *et al.* while characterizing a transposon

7

127   mutant defective in exoprotein secretion (29-32). This locus consists of an operon

128   containing the four *sae* genes, *saeP, saeQ, saeR, and saeS. saeR* encodes the DNA-

129   binding response regulator (RR) protein, and *saeS* encodes the membrane-spanning

130   sensor histidine kinase (HK) (28). *saeP* and *saeQ* encode auxiliary proteins that have

131   been shown to stimulate phosphatase activity of SaeS toward SaeR~P, resetting the

132   TCS to its pre-activation state (33). The expression of these genes is driven by two

133   promoters, P1 and P3. The P1 promoter is inducible and controls the transcription of the

134   entire *sae* operon, while the P3 promoter located in *saeQ* drives constitutive expression

135   of *saeR* and *saeS* (34). SaeS activity is triggered by neutrophil-produced factors, most

136   notably human neutrophil peptides (HNP1-3) by an unknown mechanism (35). In

137   response, SaeS autophosphorylates its conserved histidine residue. Then, SaeR is

138   phosphorylated using the phosphohistidine of SaeS as a substrate, resulting in signal

139   transduction (36, 37). This generates SaeR~P, which binds to site-specific sequences to

140   promote transcription of the target genes (38, 39). One target of SaeR~P is the *sae*P1

141   promoter. This creates a positive feedback loop, resulting in signal amplification and

142   preventing Sae activity from becoming excessive.

143

144   In canonical TCSs, the HK is capable of receiving input signals through a large

145   extracytoplasmic input domain. In contrast, SaeS lacks this domain, and the

146   extracellular-facing portion of the protein comprises only a 9 amino acid linker (40). As a

147   result, SaeS is nontraditional sensor HK and is considered a member of the

148   intramembrane family of sensor histidine kinases (IM-HK) (41). How SaeS responds to

149   HNPs is an open question. Even at a more foundational level, our knowledge of how IM-

150   HKs like SaeS function is incomplete (42-44). Herein, we report that disrupting *de novo*

151   pyrimidine biosynthesis reduces Sae-dependent promoter activity under pyrimidine-

152   limited conditions. Using PhosTag electrophoresis we determine that pyrimidine

153   limitation reduces SaeS kinase activity. This effect depends on the N-terminal

154   membrane-spanning domain of SaeS, suggesting that pyrimidines act at the membrane

155   to promote Sae kinase activity. Consistent with known roles of pyrimidine nucleoside

156   triphosphates in cell membrane and envelope biogenesis, we show that pyrimidine

157   limitation results in a thicker cell wall, irregular membrane, and an accumulation of free

158   fatty acids. Removal of free fatty acids by providing an extracellular sink for these lipids

159   is sufficient to restore Sae activity during pyrimidine limitation. The ripple effects

160   generated by defects in pyrimidine metabolism highlight the critical roles that central

161   metabolic pathways play in maintaining cellular homeostasis and virulence potential in

162   *S. aureus*, making pyrimidine biosynthesis a promising target for the development of

163   novel anti-virulent therapeutics.

164

165

Results

Disruption of *pyrE* reduces basal Sae TCS activity and pyrimidine auxotrophy.

As a member of the IM family, little is known how SaeS perceives its signals. To gain

insight on how SaeS functions mechanistically, we conducted a transposon

mutagenesis screen using a pMA15 plasmid system (45) to identify factors required for

SaeS kinase activity. Using this screen, we isolated a transposon insertion in the gene

encoding orotate phosphoribosyltransferase (*pyrE*), a critical enzyme for *de novo*

pyrimidine biosynthesis (**Fig. 1A**). To indirectly measure Sae activity, we introduced a

Sae-dependent transcriptional reporter (*sae*P1-*gfp*) into *S. aureus* strains and grew the

cells to stationary phase (16 h) in rich, complex medium (tryptic soy broth; TSB)*.* As

expected, we detected essentially no promoter activity in the Δ*sae* mutant. We

measured a 4-fold drop in promoter activity in the *pyrE::tn* mutant relative to the parent

strain (**Fig. 1B**). To confirm that the *sae* defect was associated with disruption of *pyrE*

and to eliminate the possibility of polar effects on SAUSA300_1099 immediately

downstream (annotated to encode YqzH; function unknown; depicted as *1099* in **Fig.**

1A)*,* we generated a Δ*pyrE* in-frame deletion mutant. The Δ*pyrE* mutant also showed

the same reduction in Sae activity (**Fig. 1B**). We note that the Sae system is still

capable of being activated by human neutrophil peptides (**Fig. S1**). Consistent with what

is known about the role of PyrE in the *de novo* pyrimidine biosynthetic pathway in other

Gram-positive and Gram-negative genera, the Δ*pyrE* mutant is a pyrimidine auxotroph

and is unable to grow in chemically defined medium (CDM) unless exogenous

pyrimidines like uracil are provided (**Fig. 1A and C**) (11-15, 46). Notably, the Δ*pyrE*

mutant exhibited a significant growth yield defect in addition to the Sae defect when

10

189   grown in TSB (**Fig. S2**). This strongly suggests that pyrimidines become limiting in this

190   medium and indicates that *S. aureus* relies on the *de novo* pathway to support growth in

191   TSB. As expected, pyrimidine auxotrophy (or limitation) can be chemically

192   complemented with the addition of exogenous uracil in both CDM and TSB

193   circumventing the need for *de novo* synthesis (**Fig. 1A, 1C, and S2**). Overall, these data

194   suggest a link between pyrimidine sufficiency and basal Sae activity.

195

196   **Pyrimidine limitation leads to a reduction in basal SaeS kinase activity.**

197   As mentioned previously, pyrimidines are either synthesized through the *de novo*

198   pathway as needed or taken into the cell through the pyrimidine salvage pathway to

199   support growth. Disrupting *de novo* pyrimidine biosynthesis can result in a buildup of

200   pyrimidine metabolite precursors and alter expression of the genes predicted to be

201   involved in the *de novo* and salvage pathways (14, 15). While characterizing the effects

202   of pyrimidine metabolism on regulation of the Sae TCS in *S. aureus*, we noticed that the

203   Δ*pyrE* mutant accumulates white, crystalline material extracellularly when grown on

204   TSB agar plates (data not shown). Further, Δ*pyrE* mutant strains of other bacterial

205   species accumulate orotate crystals extracellularly, and in some species this is linked to

206   defects in virulence factor production (14, 15). Therefore, we hypothesized that a

207   pyrimidine-specific metabolite, when it accumulates intracellularly or extracellularly,

208   reduces Sae TCS activity. To test this hypothesis, we constructed additional mutations

209   along the *de novo* pathway and measured *sae*P1 promoter activity as a proxy for Sae

210   activity. Interestingly, when we deleted the genes annotated to encode dihydroorotate

211   dehydrogenase (*pyrD*) and dihydroorotase (*pyrC*)*,* we measured essentially the same

11

212 low *sae*P1-*gfp* promoter activity as that measured in the *pyrE* mutant strains (**Fig. 1B**

213 **and 2A**). The Sae activity defect in these strains could be complemented chemically by

214 supplementing exogenous uracil or cytidine, or genetically in the Δ*pyrD* mutant by

215 ectopically expressing a wild-type copy of *pyrD*⁺ under control of its native promoter

216 (**Fig. 2A and S3)**. Although we could have tested the effects of mutations further up the

217 *de novo* pathway, we opted not to as to avoid further interference with other biosynthetic

218 pathways (47). Since we observed an identical reduction in Sae activity in the Δ*pyrD*

219 and Δ*pyrC* mutant cells relative to the Δ*pyrE* mutant cells, we then reasoned that the

220 pyrimidine-related Sae defect is due to limitation. If so, Sae activity should be unaffected

221 during exponential phase prior to the onset of pyrimidine limitation. To test this, we

222 collected cells that were growing exponentially in TSB (2 h) and monitored Sae activity

223 using *sae*P1-*gfp*. Consistent with our complementation data, both the *pyrE::tn* and

224 Δ*pyrE* mutants showed no Sae defect when levels of pyrimidine in the medium were not

225 limiting (**Fig. 2B**). Taken together, our data suggest that the defect in basal Sae activity

226 is not due to buildup of metabolites, but rather due to pyrimidine limitation itself.

227

228 Unphosphorylated SaeR cannot bind to target promoters to stimulate gene transcription

229 (39). Only activated SaeR (SaeR~P) can bind. Because there is little to no crosstalk

230 between HKs and RRs, Sae output (i.e., target gene promoter activity) is solely

231 dependent on the activity of SaeS (48). To test the hypothesis that pyrimidine limitation

232 affects SaeS kinase activity directly, we used Phos-Tag electrophoresis (49) and

233 Western blotting with polyclonal antibodies raised against SaeR to measure relative

234 levels of SaeR SaeR species in Δ*pyrE* mutant cells during pyrimidine-limited and

235   pyrimidine-replete conditions. During exponential phase, we detected slightly higher

236   levels of SaeR in the ΔpyrE mutant relative to WT, but we were unable to detect

237   SaeR~P in either sample. This is consistent with previous studies reporting very low

238   levels of Sae activity during this period (50, 51). Notably, we measured a general

239   reduction in total SaeR protein levels and a concomitant drop in the fraction of SaeR~P

240   in the ΔpyrE mutant cells during pyrimidine limitation (**Fig. 2 C-F**). Given that SaeR

241   levels are dependent in part on the activity of SaeS through SaeR~P-mediated

242   activation of the P1 promoter, this may confound our analysis, giving us a false sense

243   that SaeR~P levels are lower in the ΔpyrE mutant. To compare SaeS kinase activity

244   directly without confounding autoregulation, we complemented Δsae and Δsae ΔpyrE

245   mutant strains with either *saeRS* (+*RS*) ectopically expressed under the control of the

246   constitutive P3 promoter or the empty vector (+EV) and remeasured SaeR~P as a

247   percentage of the total SaeR in these cells. As expected, we measured no difference in

248   total SaeR levels in ΔpyrE mutant cell lysates compared to WT cell lysates. Notably, we

249   observed a dramatic reduction in the fraction of SaeR~P in the ΔpyrE mutant cell

250   lysates (**Fig. 3A-C**). Taken together, these data indicate that pyrimidine limitation results

251   in a reduction of SaeS kinase activity.

252

253   **The N-terminal, membrane-spanning domain of SaeS is the site of regulation of**

254   **the Sae TCS by pyrimidines.**

255   The prevailing view is that the overall conformation of the N-terminal domain is critical

256   for controlling kinase activity. To test if the N-terminal domain hinders the kinase activity

257   of SaeS in ΔpyrE mutant cells during pyrimidine limitation, we measured SaeS kinase

13

258   activity in strains producing either full-length SaeS or just the catalytic, C-terminal

259   kinase domain located in the cytosol (SaeSc). We found that the *sae*P1-*gfp* fusion was

260   no longer affected by pyrimidine limitation. In fact, we noted a significant increase in

261   promoter activity compared to that measured in otherwise WT cells producing full length

262   SaeS when SaeSc is produced (**Fig. 3D)**. Consistent with this observation, overall SaeR

263   levels were increased in addition to the ratio of SaeR~P/SaeR species in the Δ*pyrE*

264   mutant during limitation (**Fig. S4**). These data indicate that pyrimidine limitation

265   specifically targets the N-terminal membrane-spanning portion of SaeS, reducing kinase

266   activity.

267

268   **Pyrimidine limitation significantly alters the transcriptome of Δ*pyrE* mutant cells.**

269   Given that the Sae defect in the Δ*pyrE* mutant cells during pyrimidine limitation is

270   associated with the N-terminal membrane-spanning domain of SaeS, we wondered if

271   pyrimidine limitation is generally linked to a defect in the envelope environment. If this is

272   true, then the effect of pyrimidine limitation likely extends beyond Sae to many proteins

273   in the membrane, several of which are kinases for other TCSs. To determine the full

274   extent to which pyrimidine limitation alters gene expression and help inform a potential

275   mechanism for Sae activation, we performed transcriptional profiling in wild-type and

276   isogenic Δ*pyrE* mutant cells grown to early stationary phase (i.e., pyrimidine-limiting

277   conditions). Overall, we noticed that the transcriptome was dramatically altered in the

278   Δ*pyrE* mutant cells during limitation, with 701 genes significantly downregulated and

279   719 genes significantly upregulated (Log$_2$ fold change ≥ 1 or ≤ -1 and *p*<0.05;

280   Δ*pyrE*/WT) (**Table S1**). This dramatic shift in the transcriptional profile of the Δ*pyrE*

281   mutant likely stems from the interconnectedness of pyrimidine metabolism with other

282   central metabolic pathways and various regulators in the cell (13, 52). To determine

283   whether pyrimidine limitation affects specific pathways preferentially, we performed

284   KEGG enrichment analysis on the RNA-seq output using KEGGREST with the

285   USA300_FPR3757 KEGG reference genome (KEGG;saa) (53, 54). Based on KEGG

286   enrichment, the majority of differentially expressed genes (DEGs) annotated to be

287   involved in 80 different KEGG pathways were downregulated in the Δ*pyrE* mutant cells

288   during pyrimidine limitation (**Table S2**). This includes directly regulated pathways such

289   as purine metabolism, various pathways involved in cell envelope biogenesis (e.g., fatty

290   acid biosynthesis, teichoic acid biosynthesis, and peptidoglycan biosynthesis), and the

291   various sugar related metabolic pathways. Further, based on this analysis, it indicates

292   that 46 out of the 53 DEGs encoding proteins annotated to be involved in TCS signaling

293   are downregulated in the Δ*pyrE* mutant relative to WT during pyrimidine limitation. Since

294   the KEGG pathways base gene annotation off of functionally similar genes in previously

295   reported systems (55), this may lead to overestimation of the effect on TCSs and

296   prompts us to look closer into the pyrimidine limitation-induced impact on the various

297   TCSs. To begin to answer this question, we took advantage of the fact that TCSs exhibit

298   feedback autoregulation of the HK and RR to indirectly assess the overall impact on

299   kinase activity of the other 15 TCSs (56, 57). We saw that, in addition to the $\log_2$-fold

300   drop in *saeRS* transcripts, there was a general reduction in the expression of the other

301   TCS coding genes in the Δ*pyrE* mutant cells during pyrimidine limitation (**Table 1**).

302   Interestingly, the Agr quorum sensing TCS had the highest reduction in expression

303   relative to the other systems with a 5- to 6- fold drop in *agrCA* transcript abundance.

304   Since AgrC has a lower affinity for ATP (58) and ATP is required to activate the sensor

305   kinases of the TCSs, we wondered if the reduction in activity of these TCSs was

306   potentially correlated with a drop in intracellular ATP pools due to a concomitant

307   reduction of purine biosynthesis in the Δ*pyrE* mutant cells during pyrimidine limitation.

308   Although we did not test the effect of pyrimidine limitation on purine biosynthesis

309   specifically by measuring ATP pools, KEGG analysis identified that 21 of the 29 DEGs

310   were downregulated for purine biosynthesis. Further, 10 of the 14 genes previously

311   annotated to be involved in the *de novo* purine biosynthetic pathway and all of the

312   genes annotated for the different subunits of the ATP synthase were significantly

313   downregulated in the Δ*pyrE* mutant during pyrimidine limitation (**Table 2 and S2**). This

314   suggests that the cell is reducing purine production in response to pyrimidine limitation

315   to maintain balance within the cell. In addition, many of the genes annotated to be

316   involved in nucleotide salvage were upregulated in the Δ*pyrE* mutant cells (**Table 2**).

317   Collectively, these data show that defective pyrimidine metabolism results in a global

318   change to the transcriptional profile of *S. aureus* when pyrimidines are limited, including

319   those involved in the synthesis of envelope components. Further, transcriptomic

320   analysis suggests that pyrimidine limitation generally reduces the kinase activity of the

321   majority of TCSs in Δ*pyrE* mutant cells.

322

323   **Pyrimidine limitation is associated with cell wall thickening and an unstable**

324   **membrane.**

325   Up to this point, we have shown that SaeS integrates pyrimidine sufficiency to regulate

326   basal kinase activity via the membrane-spanning domain. However, how pyrimidine

16

327   sufficiency is perceived by SaeS mechanistically remains unknown. Because pyrimidine

328   nucleotides are used to activate precursors for peptidoglycan, teichoic acid, and

329   phospholipid synthesis and that genes that direct the synthesis of these membrane

330   constituents are differentially expressed, we reasoned that during pyrimidine limitation a

331   modified cell envelope might contribute to the defect in SaeS kinase activity. We

332   determined the minimum inhibitory concentration (MIC) of the ΔpyrE mutant and the WT

333   parent strain for available molecules that target synthesis of major cell envelope

334   components (59). We measured no change in susceptibility to fosfomycin (first

335   committed step in peptidoglycan synthesis), tunicamycin (wall teichoic acid synthesis),

336   or oxacillin (peptidoglycan crosslinking) (**Table S3**) (59-62). In contrast, we observed a

337   4- to 8-fold increase in the susceptibility to congo red, with a change in MIC from 0.25%

338   in WT cells to 0.06%-0.03 in ΔpyrE mutant cells. Congo red was previously reported to

339   be an inhibitor of LtaS (lipoteichoic acid [LTA] synthase) that is critical for LTA assembly

340   (63). To better understand the change in susceptibility, we extracted lipoteichoic acids

341   from WT and ΔpyrE mutant cells and found that the ΔpyrE mutant has increased

342   production of LTAs (**Fig. S5AB**). Previously, uncontrolled LTA synthesis in the absence

343   of the small membrane regulatory protein MspA was shown to result in virulence defects

344   (64, 65). To determine whether pyrimidine limitation acts in the same regulatory

345   pathway as MspA we performed a genetic epistasis experiment. The *mspA::tn* single

346   mutant showed essentially the same SaeS kinase activity defect as the ΔpyrE mutant,

347   as judged by phos-tag experiments. No further reduction in kinase activity was

348   measured in the ΔpyrE mspA::tn double mutant. The kinase defect was complemented

349   when a wild-type copy of *mspA*$^+$ was provided *in trans* in the *mspA::tn* single mutant,

17

350   but not in the Δ*pyrE mspA::tn* double mutant, suggesting that the effects on Sae activity

351   are independent from one another (**Fig. S5C**).

352

353   To get a better understanding on the impact of pyrimidine limitation on the cell

354   envelope, we performed transmission electron microscopy (TEM) on WT, Δ*pyrE*, and

355   Δ*pyrE* mutant cells fed exogenous uracil. Multiple observations are consistent with an

356   abnormal cell envelope. First, Δ*pyrE* mutant cells experiencing pyrimidine limitation are

357   nearly twice as large as WT cells; this phenotype is complemented when the missing

358   nutrient is provided (**Fig. S6 A-D**). Second, Δ*pyrE* mutant cells under limitation

359   conditions have a much thicker cell envelope and a visibly crenulated membrane

360   architecture relative to WT or the chemically complemented cells (**Fig. 4A-D**). Increased

361   envelope thickness in the Δ*pyrE* mutant is consistent with the idea that defects in central

362   metabolism and/or increased LTA biosynthesis result in thickening of the cell envelope

363   (11, 61, 64). In addition to the dramatic difference in membrane morphology between

364   WT and pyrimidine-limited (Δ*pyrE* mutant) cells, Δ*pyrE* mutant cells accumulated more

365   of the eponymous staphyloxanthin pigment compared to wild-type cells (**Fig. S7A**).

366   Because increased incorporation of staphyloxanthin in the membrane has been shown

367   to rigidify the membrane (66, 67), we wondered if this increased staphyloxanthin

368   incorporation was restraining SaeS kinase activity. To test this, we utilized an available

369   transposon mutant in *crtM* encoding the 4,4'-diapophytoene synthase that is critical for

370   staphyloxanthin synthesis (*crtM::tn*) and measured *sae*P1-*gfp* promoter activity in the

371   *crtM::tn* single mutant and the Δ*pyrE crtM::tn* double mutant. We found that disrupting

372   *crtM* had no effect on Sae activity in either genetic background, indicating that the

18

373 increased staphyloxanthan accumulation did not explain the Sae signaling defect (**Fig.**

374 **S7B**). Rather, the increased staphyloxanthin production may be in response to the

375 irregularities we observe in the cell membrane, and an attempt to reinforce an unstable

376 membrane. Taken together, these data suggest that pyrimidine sufficiency is correlated

377 with proper cell envelope biogenesis.

378

379 **Pyrimidine sufficiency promotes SaeS kinase activity by reducing free fatty acid**

380 **levels in the membrane.**

381 Cytidine nucleosides play a central role in lipid synthesis in prokaryotes and eukaryotes

382 (68). Phosphatidate cytidylyltransferase (CdsA) condenses phosphatidic acid (PA) with

383 CTP to form activated diacylglycerol (CDP-diacylglycerol; CDP-DAG) with the

384 elimination of pyrophosphate. Displacement of CMP and cleavage of the phosphate

385 monoester yields phosphatidylglycerol (69, 70). Previous studies have reported that the

386 buildup of CDP-DAG precursors, specifically unincorporated free fatty acids (FFAs) in *S.*

387 *aureus* membranes, is shown to inhibit the Sae TCS (71, 72). We reasoned that low

388 CTP levels during pyrimidine limitation would reduce CdsA activity and lead to

389 increased incorporation of FFAs into the membrane. To test this, we grew WT and

390 Δ*pyrE* mutant cells to stationary phase (16 h) in the presence of fatty acid-free bovine

391 serum albumin (BSA) and measured *sae*P1 promoter activity. BSA has been shown to

392 bind and remove FFAs from the cell membrane, providing an extracellular sink for these

393 lipids and reviving Sae TCS activity (43, 71-73). As expected, BSA treatment resulted in

394 a modest increase in Sae activity in WT cells. Surprisingly, BSA treatment restored Sae

395 activity to WT levels in the Δ*pyrE* mutant (**Fig. 5A**). We note that BSA addition did not

396   restore pyrimidine auxotrophy of the mutant when grown in CDM (data not shown). A

397   two-fold increase in BSA concentration had no further effect on Sae activity (**Fig. S8A**).

398   LC-MS/MS analysis of supernatant samples revealed differences in the abundances of

399   specific FFAs recovered using BSA treatment (**Fig. 5B**). Interestingly, we noticed that

400   there was a dramatic increase in the abundance of 13:0 FFAs and a moderate increase

401   in the abundance of 20:0, 22:0, and 24:0 FFAs recovered from the media from WT and

402   Δ*pyrE* mutant cultures treated with BSA, where Sae activity is restored, relative to the

403   untreated controls (**Fig. 5AB**). Of the FFAs identified, the 13:0 species seemed to be

404   the highest FA in abundance in the media from both the WT and Δ*pyrE* mutant cells

405   treated with BSA. However, it is unclear if 13:0 is limiting Sae activity. Even though LC-

406   MS/MS allows us to identify FFA species, we cannot distinguish between different

407   isoforms of the fatty acids detected. Given that anteiso branched-chain fatty acids

408   derived from isoleucine (*a*15:0) promotes Sae activity (43, 44), we wondered if adding

409   this fatty acid would rescue Sae activity in the Δ*pyrE* mutant as it is dramatically

410   reduced in the supernatants of Δ*pyrE* mutant cultures during limitation. As expected,

411   exogenous *a*15:0 restored Sae activity in a strain depleted for this membrane fatty acid

412   (*lpdA::tn mbcS1*) (43, 44, 74). To our surprise, the addition of exogenous *a*15:0 led to a

413   further reduction of Sae activity in the Δ*pyrE* mutant cells (**Fig. S8B**). There was no

414   additional effect of *a*15:0 addition on growth. These data support the idea that the

415   SaeRS defect seen in Δ*pyrE* mutant cells stems from FFA accumulation in the

416   membrane due to a pyrimidine limitation-induced bottleneck during phospholipid

417   biosynthesis.

418

Discussion

This study aligns with the idea that nucleotide metabolism is an important factor for regulating virulence in *S. aureus* among other pathogens. Previous work from our lab and others have shown that mutations in *de novo* purine biosynthesis are correlated with altered expression of the virulence regulatory network (75-77). Specifically, mutations in the GMP synthase (GuaA) result in increased activity of the AgrCA TCS and enhanced protease activity *in vitro*. Further, it has been shown that the purine biosynthesis regulatory protein, PurR, can moonlight as a virulence regulator and represses expression of fibronectin binding proteins and extracellular toxins *in vivo* and *in vitro* (75, 78). On the contrary, mutations in *de novo* pyrimidine biosynthesis are correlated with a reduction in expression of virulence factors *in vitro* and *in vivo*. One study specifically looked at the impact of a mutation in the thymidylate synthase, ThyA, which was which downstream of the *de novo* pathway and is responsible for the conversion of deoxy uridine monophosphate (dUMP) into thymidylate (dTMP) (11). They report that defective thymidylate synthesis is associated with a dramatic reduction *S. aureus* virulence *in vitro* and *in vivo* (11). Interestingly, regardless of the effects of purine and pyrimidine metabolism on enhancing or reducing virulence *in vitro*, *S. aureus* must be able to synthesize nucleotides *de novo* to support and maintain proper envelope homeostasis and the various cellular processes for proliferation within the otherwise nucleotide desert that is the host environment. This dual role of nucleotide metabolism in supporting both staphylococcal fitness and virulence makes it particularly attractive for the development of novel therapeutics. Thus, using an inhibitor that targets the *de novo* purine or pyrimidine biosynthetic would significantly hinder bacterial fitness

21

442   and put the bacterium in a situation where the virulence regulatory systems could not

443   function properly, ultimately leading to host clearance. Although purine and pyrimidine

444   metabolism have been considered determinants for virulence potential, there is little

445   mechanistic information about how these critical pathways contribute to virulence

446   regulation. Here, we propose a model where pyrimidines act indirectly on the activity of

447   the SaeRS TCS in *S. aureus* by maintaining membrane homeostasis (**Fig. 6**).

448   Moreover, this study provides a unique perspective on the importance of membrane

449   homeostasis and offers insight into how these IM-HKs, such as SaeS, are regulated.

450

451   To determine the mechanistic basis for the role of pyrimidine sufficiency in regulating

452   the activity of the SaeRS TCS, the first task was to distinguish between metabolite

453   accumulation and pyrimidine limitation as the root cause. Based on what is known about

454   the role of orotate in regulating virulence in other organisms (15, 79), we initially

455   hypothesized orotate or other pyrimidine metabolites were antagonizing Sae activity.

456   Although we observed orotate crystal formation in the Δ*pyrE* mutant colonies on solid

457   medium, we determined that the defect was not due to orotate accumulation as the

458   Δ*pyrD* and Δ*pyrC* mutants, which do not accumulate orotate and dihydroorotate,

459   phenocopy the Δ*pyrE* mutant (**Fig. 2A**). Further, Sae activity is unaffected in pyrimidines

460   replete conditions, consistent with the hypothesis that the defect is caused by pyrimidine

461   limitation (**Fig. 2B**). We note that we cannot exclude the possibility that providing

462   exogenous pyrimidines represses the *pyr* genes, preventing the accumulation of an

463   inhibitory metabolite up stream of PyrC in the pathway. Moreover, it has been shown

464   that purine and pyrimidine metabolism directly influence the activity of their respective

465   pathways primarily through feedback inhibition of the regulatory proteins, PurR and

466   PyrR. Although these two proteins have distinct regulatory mechanisms, they both

467   function by sensing final or intermediate products of the pathways to control the

468   expression of genes involved in nucleotide biosynthesis, thereby maintaining nucleotide

469   balance within the cell (80). Given that feedback inhibition occurs, we were not

470   surprised to see that most genes involved in purine biosynthesis were downregulated,

471   while the genes encoding putative proteins involved in the *de novo* pyrimidine

472   biosynthetic pathway (*pyrB*, *pyrC*, and *pyrD*) were upregulated in the Δ*pyrE* mutant

473   during pyrimidine limitation (**Table 2; Table S2; Fig. 1A**). This underscores the

474   influence that each respective biosynthetic pathway has on one another.

475

476   Our findings suggest pyrimidines affect SaeS through its N-terminal membrane-

477   spanning domain, which is consistent with previous work showing IM-HKs like SaeS are

478   sensitive to membrane composition changes (43, 44, 71, 72, 81). This is evidenced by

479   the absence of pyrimidine-dependent Sae activity defects when complementing a Δ*sae*

480   Δ*pyrE* mutant with a truncated SaeS lacking its membrane-spanning domain (**Fig. 3**

481   **and S4**). In addition to identifying the connection of the Sae phenotype to the

482   membrane, this experiment ruled out the possibility that reduced ATP pools were to

483   blame for the low Sae activity. We also note that the expression of SaeR in the Δ*sae*

484   Δ*pyrE* mutant cells complemented with the *sae*P3-*saeRSc* construct was enhanced

485   relative to the new WT control (Δ*sae* + *RSc*). Several possibilities could explain this

486   unexpected result. First, the difference in expression may stem in issues with ectopic

487   expression of these constructs at a different locus. Second, this may be due to

488   increased stability of SaeR in the Δ*pyrE* mutant background, possibly through

489   decreased degradation by reduced activity of the Clp proteases. Third, the single

490   mutant expressing the *sae*P3-*saeRSc* construct is the anomalous result, and the

491   heightened activity seen in the Δ*pyrE* mutant is the expected result based on previous

492   work with showing heightened Sae activity in the otherwise WT background (40).

493   Regardless of expression and stability of the proteins, there is still a dramatic

494   enhancement in the overall kinase activity of SaeSc when expressed in the Δ*pyrE*

495   mutant background (**Fig. S4**). Further work is needed to dissect the root cause of this

496   difference in expression profiles of the P3*saeRSc* construct.

497

498   We observed dramatic changes to the cell wall architecture when pyrimidines are

499   limited. Our observations are consistent with other reports that show defects in central

500   metabolism result in an altered cell envelope (11, 43, 44, 61, 74, 77). Since the MICs for

501   envelope-targeting drugs remained largely unchanged beyond the effects on LTAs in

502   ΔpyrE mutant cells under limitation, and the SaeS kinase defect is linked to its N-

503   terminal membrane domain, our findings suggest that envelope alterations create an

504   environment unfavorable for full SaeS kinase activity. Previous studies showed that

505   unchecked LTA synthesis results in a virulence defect but did not measure the activities

506   of the major virulence regulatory systems AgrCA and SaeRS (64, 65). Both the LTA and

507   phospholipid biosynthetic pathways share diacylglycerol (DG) as a common

508   intermediate. Our data suggest that the accumulation of LTA in the Δ*pyrE* mutant may

509   be the result of diverting metabolic flux from phospholipid synthesis to LTA synthesis

510   (**Fig. S5**)(82). Accumulation of LTA in the Δ*pyrE* mutant background may help the cells

24

511   compensate for the defect in phospholipid biosynthesis as LTAs serve important roles in

512   processes associated with the envelope including ion homeostasis, maintaining proton

513   motive force, as well as regulating autolysin activity (83, 84). In this study we also

514   discovered that increased LTA synthesis is associated with a defect in SaeS kinase

515   activity. This is consistent with a prior study that reported the link between *mspA* and

516   Sae-dependent virulence factors (65). However, during pyrimidine limitation, increased

517   LTA synthesis does not seem to be responsible for the Sae defect. Our observation that

518   LTAs affect Sae is nevertheless important to note. How might this work? It is

519   conceivable that SaeS may sense changes in envelope charge. LTAs are decorated

520   with various negatively charged sugars. Incorporating D-alanine allows the bacterium to

521   modify the envelope charge as a way to protect itself from host-mediated killing,

522   resulting in a more positively charged envelope (63, 82). Increased LTA incorporation

523   might alter envelope charge if D-alanylation machinery (*dlt*) cannot accommodate the

524   higher LTA flux, thus creating an unfavorable environment for maintaining SaeS activity

525   (83, 84). If so, overexpressing either *mspA* or the *dlt* may rescue of Sae activity when

526   LTA production and/or envelope charge is altered. However, more work is needed to

527   dissect the connection between LTAs and SaeS.

528

Materials and Methods

Bacterial strains and growth conditions.

Staphylococcus aureus strains used in this study are listed in **Table S4**. Unless

otherwise noted, indicated *S. aureus* strains were cultured in tryptic soy broth (TSB)

containing 0.25% (wt/vol) dextrose (BD Biosciences) or chemically defined medium

(CDM, pH 6.5) lacking pyrimidine nucleotides as previously described. Briefly, CDM

medium was formulated with alanine (672 µM), arginine (287 µM), aspartic acid (684

µM), cysteine (166 µM), glutamic acid (680 µM), glycine (670 µM), histidine (129 µM),

isoleucine (228 µM), leucine (684 µM), lysine (342 µM), methionine (20 µM),

phenylalanine (240 µM), proline (690 µM), serine (285 µM), threonine (260 µM),

tryptophan (50 µM), tyrosine (275 µM), valine (684 µM), thiamine (56 µM), nicotinic acid

(10 µM), biotin (0.04 µM), pantothenic acid (2.3 µM), $MgCl_2$ (1,000 µM), $CaCl_2$ (100

µM), monopotassium phosphate (40,000 µM), dipotassium phosphate (14,700 µM),

sodium citrate dehydrate (1,400 µM), magnesium sulfate (400 µM), ammonium sulfate

(7,600 µM), and glucose (27,753 µM) (85). *Escherichia coli* strains were grown in

lysogeny broth (LB) without glucose (10 g/L tryptone, 5 g/L yeast extract, and 5 g/L

sodium chloride)(86). When necessary, media were solidified with agar (1.5% [wt/vol])

and supplemented with antibiotics or chemicals at the indicated concentrations:

ampicillin (Amp), 100 µg/mL, chloramphenicol (Cm), 5 to 10 µg/mL; erythromycin (Erm),

5 µg/ml; tetracycline (Tc), 1.5 µg/mL; kanamycin (Km), 100 µg/mL; Bovine Serum

Albumin (BSA), 10 mg/mL. When indicated, media were supplemented with exogenous

pyrimidine (Uracil) to a final concentration of 200 µM. Unless otherwise noted, all strains

were grown at 37°C.

552

I.   **TSB growth curve:** Un-supplemented overnight cultures were used to inoculate 125-mL Delong flasks containing 12.5 mL TSB ± uracil supplementation (200 μM; 10:1 flask: medium ratio) to an optical density at 600 nm (OD_{600}) of 0.05 and incubated in a water bath shaking at 250 rpm. Cell growth was monitored over 1 h increments by measuring increase in OD_{600} using an Amersham Ultraspec 2100 Pro UV-visible spectrophotometer.

II. **CDM grown curve:** Overnight cultures grown in CDM ± uracil supplementation (200 μM) were used to inoculate a 96-well plate to an OD_{600} of 0.05. To prevent uracil carryover from overnight cultures, 1 mL of cells were pelleted (13,000 x g for 1 min) and supernatants were removed. Cell pellets were washed twice with 1 mL of un-supplemented CDM before resuspension in 1 mL of un-supplemented CDM. Samples were then inoculated into fresh CDM medium ± uracil supplementation and cell density was monitored over time using a computer-controlled BioTek Synergy H1 plate reader (BioTek/Aligent) running Gen5 software v3.14.

Genetic techniques

Oligonucleotides used for this study were synthesized by Integrated DNA Technologies (IDT; Coralville, IA) and are listed in **Table S5**. Restriction enzymes, DNA ligases, Exonucleases, DNA polymerases, Genomic DNA isolation, and PCR cleanup kits were purchased from New England Biolabs (NEB). Plasmids were extracted from *E. coli*

27

575   using the Zyppy Plasmid Miniprep kit (Zymo). Unless indicated, plasmid constructions

576   were performed using Gibson Assembly as described previously (87, 88). The plasmids

577   used in this study are listed in **Table S6**. *E. coli* NEB 5α (NEB) was used as host for

578   plasmid constructions and all plasmids were confirmed by PCR and plasmid sequencing

579   (PlasmidSaurus) before being introduced into *S. aureus* strain RN4220 by

580   electroporation (89). Plasmid and marked mutations were moved between *S. aureus*

581   strains via Φ85-mediated mediated transduction(90).

582

583   **Plasmid Constructions**

584   (i) **pDD02.** 500 bp upstream and downstream of *pyrE* was amplified from wild-type

585   gDNA using the following primer pairs: oDD062, oDD063 (500 upstream), and

586   oDD64, oDD65 (500 downstream) with Q5 DNA polymerase (NEB). pKOR1

587   (10,374 bb) was linearized and amplified using primers oDD60 and oDD61 (91).

588   Each primer was designed to add 25 bp overlapping for later Gibson assembly.

589   The linearized vector was treated with DpnI (NEB) for 1 h at 37⁰C and cleaned up

590   using a PCR purification kit (NEB). The purified PCR products were then

591   subjected to Gibson Assembly and then transformed into *E. coli* DH5a. **pDD03**

592   **and pDD10** were constructed in a similar manner for *pyrD* and *pyrC*.

593

594   (ii) **pDD05.** *pyrD* including its native promoter region were amplified from wild-type

595   gDNA with the forward primer containing a SacI cutting site and the reverse

596   primer containing a BamHI cutting site. Both the vector backbone, pLL39, and

597   the *pyrD* insert were cut with BamHI and SacI (NEB) and treated with Quick CIP

28

598 (NEB) to dephosphorylate the ends to prevent self-ligation. After CIP treatment,

599 the products were cleaned up using a PCR purification kit (NEB). The purified

600 linearized vector and insert were ligated using T4 DNA ligase (NEB) and the

601 resulting plasmid was then transformed into *E. coli* DH5a.

602

603 **Construction of in-frame deletions**

604 Plasmids pDD02 (Δ*pyrE*), pDD03 (Δ*pyrD*), and pDD10 (Δ*pyrC*) were moved to *S.*

605 *aureus* strain LAC at the permissive temperature (30°C). Allelic exchange was

606 performed as described using *secY* antisense counterselection (91). In-frame deletion

607 alleles were verified by PCR and Sanger sequencing.

608

609 **GFP reporter assays**

610 Cells carrying reporter fusions were streaked out from frozen stocks on TSA plates

611 containing appropriate antibiotics. Single colonies were used to inoculate TSB with or

612 without supplements: 200 µM uracil, 200 µM cytidine, 10 mg/mL fatty-acid-free bovine

613 serum albumin (BSA). For growth in TSB ± uracil or cytidine, cells were grown in 3 mL

614 medium in disposable 16x125 mm borosilicate glass test tubes. For BSA treatment,

615 cells were grown with the 10:1 flask:medium ratio in DeLong flasks to stationary phase

616 (16 h). Resulting cultures were then diluted 1:5 in 1X phosphate-buffered saline (PBS)

617 to a total volume of 100 µL per well in a 96-well plate. Both OD_{600} and GFP

618 fluorescence (485 nm excitation, 535 nm emission) were read in a computer-controlled

619 BioTek Synergy H1 plate reader (BioTek/Aligent) running Gen5 software v3.14. Relative

29

620 Fluorescent Units (RFU; GFP fluorescence/OD$_{600}$) were calculated by subtracting the

621 background fluorescence of TSB and dividing by OD$_{600}$ to correct for cell density.

622

623 **Analysis of SaeS kinase activity.**

624 Separation of SaeR and SaeR~P was performed as described previously (44) using

625 12% polyacrylamide gels containing 100 µM manganese and 50 µM of the acrylamide-

626 pendant Phos-tag ligand (Wako Laboratory Chemicals). Cells were grown in TSB to mid

627 exponential phase, early stationary phase and late stationary phase (2 h, 8 h, and 18 h,

628 respectively) at 37°C at 10:1 flask to medium ratio with shaking. Cell pellets (OD$_{600}$ of 10)

629 were collected at 13,000 x g and stored at -80°C prior to analysis. Whole cell extracts

630 were obtained by resuspending cell pellets in 300 µL cell extract buffer (20 mM Tris [pH

631 7.0], 1X Protease Inhibitor Cocktail Set I (Sigma-Aldrich)) and transferred to sterile

632 screw cap tubes containing approximately 100 µL of 0.1 mm silica beads. The cells

633 were homogenized at room temperature using a Precellys 24 bead beater (Bertin

634 technologies) for 3 cycles of 6500 rpm for 30 s each, followed by 3 min pauses on ice.

635 The tubes were then centrifuged at 8500 x g for 15 s settle the beads, and the

636 supernatant was transferred into new tubes. Whole-cell extracts were normalized by

637 protein concentration (absorbance at 280 nm [A280]) to 100 µg and electrophoresed on

638 Phos-tag gels with standard running buffer (0.1% [wt/vol] SDS, 25 mM Tris-HCl pH 8.3,

639 192 mM glycine) at 4°C under constant voltage (150 V) for 2 h. The gels were washed

640 for 15 min with transfer buffer (25 mM Tris [pH 8.3], 192 mM glycine, 20% methanol)

641 with 1 mM EDTA followed by a second wash without EDTA to remove manganese ions.

642 Proteins were then transferred to 0.45 µM PVDF membranes (Cytiva). Membranes were

30

643   blocked in blocking buffer (5% [wt/vol] skim milk in Tris-Buffered Saline with Tween 20

644   (TBST) (20 mM Tris-HCl pH 7.6, 150 mM NaCl with 0.1% [wt/vol] Tween 20) for 1 h.

645   Membranes were then subjected to three brief washes in TBST and incubated with

646   polyclonal rabbit antibodies to SaeR (1.5:1,000) for 1 h. Membranes were then washed

647   three times with and incubated with StarBright Blue 700 goat anti-rabbit IgG (1:3500;

648   Bio-Rad) for 1 h. Membranes were subjected to three brief washes in TBST and signals

649   were visualized using an Amersham ImageQuant800. The densities of the SaeR~P

650   relative to total SaeR signal were determined by quantification with Multi Gauge

651   software (FujiFilm). The data are representative of three different independent

652   experiments, and a representative image is shown.

653

654   **Analysis of SaeR protein levels.**

655   The whole cell extracts, and protein concentrations described above were used to

656   visualize total SaeR levels. Briefly, 100µg of whole cell extracts were subjected to 12%

657   SDS-PAGE, and proteins were transferred to 0.45 µM PVDF membranes (Cytiva). After

658   transfer, membranes were blocked in blocking buffer for 1 h. Membranes were then

659   subjected to three brief washes in TBST and incubated with polyclonal rabbit antibodies

660   to SaeR (1.5:1,000) for 1 h. Membranes were then washed three times with and

661   incubated with StarBright Blue 700 goat anti-rabbit IgG (1:3500; Bio-Rad) for 1 h.

662   Membranes were subjected to three brief washes in TBST and signals were visualized

663   using an Amersham ImageQuant800. The densities of the SaeR signal were

664   determined by quantification with Multi Gauge software (FujiFilm). The data are

31

665   representative of three different independent experiments, and a representative image

666   is shown.

667

668   **RNA Sequencing**

669   Overnight cultures of cells grown in TSB were used to inoculate 125 ml DeLong flasks

670   containing TSB with a 10:1 flask:media ratio. Flasks were incubated in a shaking water

671   bath set to 37ºC at 250 RPM for 8 h. 2 mL cells were collected at 13,000 x g, and

672   resuspended in an equal volume of quenching solution (Ethanol:Acetone [1:1]),

673   pelleted, and stored at -80ºC until use. Cell pellets were resuspended in TRIzol and

674   transferred to sterile screw cap tubes containing approximately 100 µL of 0.1mm silica

675   beads. The cells were then homogenized at room temperature using a Precellys 24

676   bead beater (Bertin technologies) for 3 cycles of 6800 rpm for 30 s each, followed by 5

677   mins pauses on ice. The tubes were then centrifuged at 4 ºC and 13,000 x g for 1

678   minute to settle the beads. Clarified extracts were then mixed in an equivalent volume of

679   100% [v/v] ethanol. RNAs were purified using a Direct-Zol RNA Miniprep kit (Zymo

680   Research) according to manufacturer's instructions and RNA yields were determined by

681   measuring (A260/280). RNA quality was determined using a 5200 Fragment Analyzer

682   System (Aligent) and RNA-Seq libraries were generated using an Illumina Stranded

683   Total RNA kit after rRNA depletion (Ribo Zero Gold; Illumina). The resulting RNA-Seq

684   libraries were then sequenced on a HiSeq 2500 Sequencing System (Illumina).

685

686   **Differential Expression Analysis**

687   The sequencing files were processed with Trimmomatic (92). Alignment to the *S.*

688   *aureus* USA300_FPR3757 genome (NC007793; NCBI) and pairwise comparisons were

689   made using Rockhopper (Wellesley College) (93, 94). Raw RNA-seq datasets were

690   uplo

691

692   **KEGG Analysis**

693   Outputs for RNA-Seq were then processed using the KEGGREST package in R to

694   determine which biological pathways were enriched or disturbed based on the KEGG

695   input genome for the USA300_FPR3757 isolate (saa; KEGG) (53, 54).

696

697   **Antibiotic Minimum Inhibitory Concentration (MIC) measurements**

698   MIC measurements were performed according to the Clinical and Laboratory Standards

699   Institute (CLSI) methods for broth microdilution susceptibility testing of staphylococci

700   (59). Strains were grown on cation-adjusted Mueller Hinton broth (caMHB) plates

701   containing 2% NaCl at 37ºC for 24 h and 5-10 colonies were resuspended in 0.85%

702   saline before adjusting to McFarland standard 0.5 (A_{600}=0.1). The cell suspensions were

703   then diluted 1:20 in sterile 1X PBS and 300 μl was used to inoculate 3 ml media

704   containing serially diluted antibiotics or compounds (Tunicamycin, Fosfomycin,

705   Oxacillin, Congo Red). The tubes were incubated at 35ºC for 24 h and MIC values were

706   recorded as the lowest compound concentration where no growth was observed.

707

708   **Lipoteichoic acid extraction and blotting**

33

709   I.   **Extraction:** Lipoteichoic acid extraction was performed as previously described

710   (61, 64, 95). Single colonies grown on TSA plates were used to inoculate 3 mL

711   cultures in disposable 16x125 mm borosilicate glass tubes (Fisher Scientific).

712   Cells were grown to stationary phase overnight (16 h) at $37^{\circ}C$ and incubated with

713   rotation. After incubation, cells were normalized to an OD_{600} of 3 and collected at

714   7800 rpm. The supernatant was removed, and pellets were resuspended in 1 mL

715   sterile 1X PBS and transferred to screw cap tubes containing approximately 100

716   µL of 100µm glass beads. The cells were homogenized at room temperature

717   using a FastPrep-24 (MP Biomedicals) for 3 cycles of 6 m/s for 40 s each,

718   followed by a 4-minute rest. Tubes were then centrifuged at 200 x g for 1 min to

719   settle the beads and 700 µLof the supernatant was transferred into a fresh 1.5

720   mL Eppendorf tube. The tubes containing the supernatant were then centrifuged

721   at 14,000 rpm for 15 min to collect the cell debris. After centrifugation, the

722   supernatant was removed, and the remaining cell debris pellet was resuspended

723   in 80 µL 2X Laemmli sample buffer (BioRad) and incubated at $95^{\circ}C$ for 20 min.

724   After heating, samples were centrifuged at 14,000 rpm for 5 min, and the

725   supernatant was stored at $-20^{\circ}C$ until ready for western analysis.

726   II.   **Blotting:** 20 µL of the LTA extracts were run on 15% polyacrylamide gels at

727   room temperature under constant voltage (100V) until the BPB reached the

728   bottom of the gel and transferred to PVDF. After transfer, membranes were

729   blocked in blocking buffer for 1 h. Membranes were then subjected to three brief

730   washes in TBST and incubated with monoclonal mouse antibodies specific for

731   LTAs (mAB55; HycultBiotech; 1:5000). Membranes were then washed three

732   times with and incubated with StarBright Blue 700 goat anti-mouse IgG (1:3500;

733   Bio-Rad) for 1 h. Membranes were subjected to three brief washes in TBST and

734   signals were visualized using an Amersham ImageQuant800. The densities of

735   the LTA signal were determined by quantification with Multi Gauge software

736   (FujiFilm). The data are representative of three different independent

737   experiments, and a representative image is shown.

738

Staphyloxanthin analysis

740 The extraction of pigment from *S. aureus* was performed as previously described (96).

741 Single colonies grown on TSA plates were used to inoculate 3 mL cultures in disposable

742 16x125 mm borosilicate glass tubes (Fisher Scientific). Cells were grown to stationary

743 phase (24 h) at 37°C and incubated with rotation. After incubation, 1 mL of culture was

744 transferred to a 1.5 mL microcentrifuge tube and pelleted at 13,000 x g for 1 min. The

745 supernatant was removed, pellets were washed with sterile distilled water, followed by

746 re-centrifugation and removal of supernatant. Cell pellets were then resuspended in 200

747 µl of methanol followed by incubation at 55°C for 3 min in an Eppendorf ThermoMixer.

748 After incubation, the cell-methanol mixture was centrifuged at 13,000 x g to remove cell

749 debris, and the supernatant containing the pigment was transferred to a new microfuge

750 tube. To ensure total removal of pigment, the extraction was repeated, and the extracts

751 were pooled together. 100 µl of extracts were then transferred to quartz cuvettes

752 containing 900 µl methanol and mixed thoroughly by pipetting before measuring at 465

753 nm in an Amersham Ultraspec 2100 Pro UV-visible spectrophotometer. Absorbance

754 was normalized by CFU enumeration by plating serially diluted cells to TSA plates.

755

Transmission Electron Microscopy

Single colonies grown on TSA plates were used to inoculate 4 mL of TSB ± uracil

supplementation (200 µM). Cells were grown to stationary phase (16 h) at 37ºC and

incubated with rotation. After incubation, cells were pelleted in 2 mL microcentrifuge

tubes until the pellet was ~2 mm tall from the bottom of the tube. Cell pellets were then

washed three times in sterile 1X PBS (pH 7.4). Samples were then fixed overnight at

4ºC in sterile 1X PBS (pH 7.4) containing 2.5% [vol/vol] EM grade glutaraldehyde before

being processed at the Laboratory of Biological Ultrastructure at the University of

Maryland, College Park, MD. Subsequently, cells were subjected to a second fixing step

in 1% [v/v] osmium tetroxide for 1 h. Samples were then washed 3 times in double

distilled water and postfixed in 2% [v/v] uranyl acetate solution for 60 min. Samples

were then dehydrated using five incremental ethanol washes (35%, 50%, 70%, 95%,

100% [v/v] for 10 min each wash); the final wash using ethanol (100% [v/v]) was

repeated 3 times. Following dehydration, cells were infiltrated using propylene oxide

(100% [v/v]) two times for 15 min each followed by overnight incubation with agitation in

a 1:1 [v:v] mixture of propylene oxide (100% [v/v]) and resin (100% [v/v]). The following

morning, samples were subjected to incremental infiltration steps (1:2, 1:3, 100% resin;

propylene oxide (100% [v/v]): resin (100% [v/v]) for 60 min each step); the final

infiltration step with 100% resin was repeated before embedding the samples in fresh

resin. Samples were then solidified by incubating the resin at 70 ºC for a total of 12 days

before thin-sectioning and staining. Stained sections were loaded onto mesh grids for

imaging. Images were obtained on a Hitachi HT7700 Transmission Electron Microscope

778   at the Laboratory of Biological Ultrastructure at the University of Maryland, College

779   Park, MD. Cell diameter and envelope thickness were measured in FIJI (97).

780   Measurements were determined by first setting pixel values to the length of the scale

781   bar, followed by use of the line tool to measure cell diameter or envelope thickness

782   (from cell membrane to the outside of the cell wall), respectively.

783

784   **Medium free fatty acid (FFA) analysis using QTRAP 5500**

785   This method is designed to measure 21 classes of lipid molecules which includes free

786   fatty acids (FFA) using QTRAP® 5500 LC-MS/MS System (Sciex). Single colonies were

787   used to inoculate 125 mL DeLong flasks containing TSB ± BSA (10mg/mL) with a 10:1

788   flask:medium ratio. Flasks were incubated in a shaking water bath set to 37ºC at 250

789   rpm for 16 h. Resulting cultures were checked for promoter activity then pelleted at

790   3500 x g for 20 min in a sterile 50 mL falcon tube. After pelleting the cells, 9 mL of the

791   supernatant was transferred to a fresh 50mL falcon tube. For FFA analysis, 2 ml

792   supernatant from resulting promoter activity cultures was freeze dried and used for

793   sample preparation. 125 µL of pre-chilled isopropanol containing internal standard

794   (FFA-d4-Palmitic acid – 1ug per mL; Cambridge Isotope Laboratories) was added and

795   samples were vortexed. The sample tube was plunged into dry ice for 30 s followed by

796   a 90 s incubation in a 37 °C water bath. The freeze thaw cycle was repeated for three

797   times followed by sonication for 30 s. After sonication, samples were vortexed for 1 min

798   and were incubated at -20°C for overnight for complete protein precipitation. The

799   samples were then centrifuged at 13,000 rpm for 20 min at 4°C. After centrifugation, the

800   supernatant of each sample was transferred to a MS vial for LC-MS analysis. 5 µL of

801   each sample was injected onto a Xbridge amide 3.5 µm, 4.6 X 100 mm (waters) using

802   SIL-30 AC auto sampler (Shimazdu) connected with a high flow LC-30AD solvent

803   delivery unit (Shimazdu) and CBM-20A communication bus module (Shimazdu) online

804   with QTRAP 5500 (Sciex, MA, USA) operating in positive and negative ion mode. A

805   binary solvent comprising of acetonitrile/water 95/5 with 10 mM ammonium acetate as

806   solvent A and acetonitrile/water 50/50 with 10 mM ammonium acetate as solvent B was

807   used for the resolution. Lipids were resolved at 0.7 mL/min flow rate, initial gradient

808   conditions started with 100% of solvent A at 0.2 ml per min flow rate, shifting towards

809   99.9% of solvent A over a time period of 3 min, 94% of solvent A over a time period of 2

810   min at 5 min and 75% of solvent A over a period of 2 min. Finally, equilibrating to initial

811   conditions (100% of solvent A) over a time period of 3 minute using auto sampler

812   temperature 15°C and oven temperature 35°C. Source and gas setting were used as

813   follows: curtain gas = 30, CAD gas = medium, ion spray voltage = 5.5 kV in positive

814   mode and −4.5 kV in negative mode, temperature = 550 °C, nebulizing gas = 50 and

815   heater gas = 60. The data were then normalized to the respective internal standard area

816   (FFA-d4-Palmitic acid; Cambridge Isotope Laboratories) and processed using

817   MultiQuant 3.0.3 (Sciex). The quality and reproducibility of LC-MS data was ensured

818   using several measures. The column was conditioned using the pooled QC samples

819   initially and were also injected periodically to monitor shifts in signal intensities and

820   retention time as measures of reproducibility and data quality of the LC-MS data.

821

822   **Statistical analysis**

823   Data shown are the results of at least three independent experiments. Statistical

824   significance was determined using Prism ver. 10 (GraphPad) with the indicated tests.

825

Accession number

827   RNA-sequencing date have been deposited in the NCBI database under the BioProject

828   accession number PRJNA1232367 and in the Sequence Read Archive (SRA) under

829   accession number(s) (SRR32583580 through SRR32583585).

830

845   data collection and analysis, decision to publish, or preparation of the manuscript.

846

847   **Author Contributions**

848   DAD and SRB conceived the study; WY originally identified *pyrE::tn* mutant; DAD and

849   SRB conceptualized the research goals and aims; DAD performed the investigations

850   and analyzed the data, DAD and SRB prepared the original manuscript draft; DAD, WY,

851   and SRB prepared the final manuscript.

852

853 **Tables**

Gene	Log$_2$ Fold Change ($\Delta pyrE$/WT)	-log$_{10}$p	Adjusted p-value
saeS	-2.63	6.8E-19	0.00
saeR	-2.07	7.8E-07	0.00
agrC	-5.03	1.2E-307	0.00
agrA	-6.15	1.2E-307	0.00
airS	1.35	9.8E-08	0.00
airR	0.24	5.6E-01	1.00
vraS	-1.08	1.2E-04	0.00
vraR	-1.70	2.0E-15	0.00
phoR	-2.18	5.0E-16	0.00
phoP	-2.06	2.7E-16	0.00
desK	-0.36	3.4E-01	1.00
desR	-0.85	1.4E-03	0.00
arlS	-1.71	1.6E-10	0.00
arlR	-0.87	4.5E-03	0.01
braS	-1.21	7.8E-05	0.00
braR	-0.25	4.8E-01	0.87
graS	-1.25	1.5E-06	1.00
graR	-0.16	6.0E-01	1.00
hptS	-1.39	1.8E-10	1.00
hptR	-2.32	2.1E-45	1.00
hssS	0.44	1.0E-01	1.00
hssR	2.06	1.4E-14	1.00
kdpD	-3.17	1.4E-161	1.00
kdpE	-3.22	3.9E-187	1.00
lytS	0.78	7.5E-03	1.00
lytR	0.00	9.7E-01	1.00
nreB	-1.90	1.9E-14	0.00
nreC	-2.40	4.5E-44	0.00
srrB	0.23	3.0E-01	0.58
srrA	-0.56	4.5E-02	0.10
walK	-0.65	3.7E-02	0.08
walR	0.84	4.3E-03	0.01

854 **Table 1: Pyrimidine limitation negatively effects expression of most two-**

855 **component systems in the $\Delta pyrE$ mutant**

41

856 RNA-seq analysis results quantifying the fold-change in expression of TCS HK and RR

857 genes in the Δ*pyrE* mutant relative to the WT after 8 h of growth in TSB (pyrimidine-

858 limiting condition for Δ*pyrE* mutant cells). Raw reads were trimmed using Trimmomatic.

859 Trimmed reads were aligned and analyzed based on the reference genome (USA300

860 FPR3757; NC007793) using Rockhopper. p-values were determined using a Negative

861 Binomial distribution and adjusted p-values were determined using the Benjamin

862 Hochberg procedure built into the script. The full data set can be found in **Table S1**.

863

Pyrimidine Biosynthesis and Salvage			
Gene	Log$_2$ Fold Change ($\Delta pyrE$/WT)	-log$_{10}$p	Adjusted p-value
nupC	1.12	3.08E-04	0.00
pyrR	4.47	1.15E-307	0.00
pyrP	3.82	9.07E-306	0.00
pyrB	1.91	1.50E-16	0.00
pyrC	0.69	1.56E-01	0.32
carA	0.16	5.38E-01	0.95
carB	-0.65	1.48E-01	0.30
pyrF	-1.23	8.51E-05	0.00
pyrE	----	1.15E-307	0.00
pyrH	1.63	1.49E-10	0.00
cdd	-0.80	5.79E-03	0.01
udk	0.99	7.62E-04	0.00
upp	-2.00	1.02E-12	0.00
pyrG	-0.70	6.45E-02	0.14
pdp	-1.30	1.49E-04	0.00
pyrD	3.79	1.15E-307	0.00
Purine Biosynthesis and ATP Synthesis			
Gene	Log$_2$ Fold Change ($\Delta pyrE$/WT)	-log$_{10}$p	Adjusted p-value
purA	-0.31	5.83E-01	1.00
purR	-0.61	4.38E-02	0.10
purE	-1.16	8.60E-05	0.00
purK	-2.56	4.73E-32	0.00
purC	-3.63	2.08E-255	0.00
purS	-4.27	1.15E-307	0.00
purQ	-5.37	1.15E-307	0.00
purL	-6.91	1.15E-307	0.00
purF	-7.76	1.15E-307	0.00
purM	-8.16	1.15E-307	0.00
purN	-8.63	1.15E-307	0.00
purH	-7.43	1.15E-307	0.00
purD	-7.51	1.15E-307	0.00
purB	0.34	4.57E-01	0.83
atpC	-5.10	1.15E-307	0.00
atpD	-4.83	1.15E-307	0.00
atpG	-4.99	1.15E-307	0.00
atpA	-4.38	1.15E-307	0.00
atpH	-3.86	1.15E-307	0.00

864
865
866
867
868

atpF	-3.48	1.27E-185	0.00
atpA	-4.38	1.15E-307	0.00
atpE	-2.59	1.27E-46	0.00
atpB	-1.87	1.04E-09	0.00

869 **Table 2: Pyrimidine limitation results in differential expression of genes involved**

870 **in purine and pyrimidine biosynthesis in the Δ*pyrE* mutant**

871 RNA-seq analysis results quantifying the fold-change in expression of annotated purine

872 and pyrimidine biosynthesis genes as well as the annotated ATP synthase genes in the

873 Δ*pyrE* mutant relative to the WT after 8 h of growth in TSB (pyrimidine-limiting condition

874 for Δ*pyrE* mutant cells). Raw reads were trimmed using Trimmomatic, trimmed reads

875 were aligned and analyzed based on the reference genome (USA300 FPR3757;

876 NC007793) using Rockhopper. p-values were determined using a Negative Binomial

877 distribution and adjusted p-values were determined using the Benjamin Hochberg

878 procedure built into the script. The full data set can be found in **Table S1**.

879

880

881

882

883   **Figures**

884
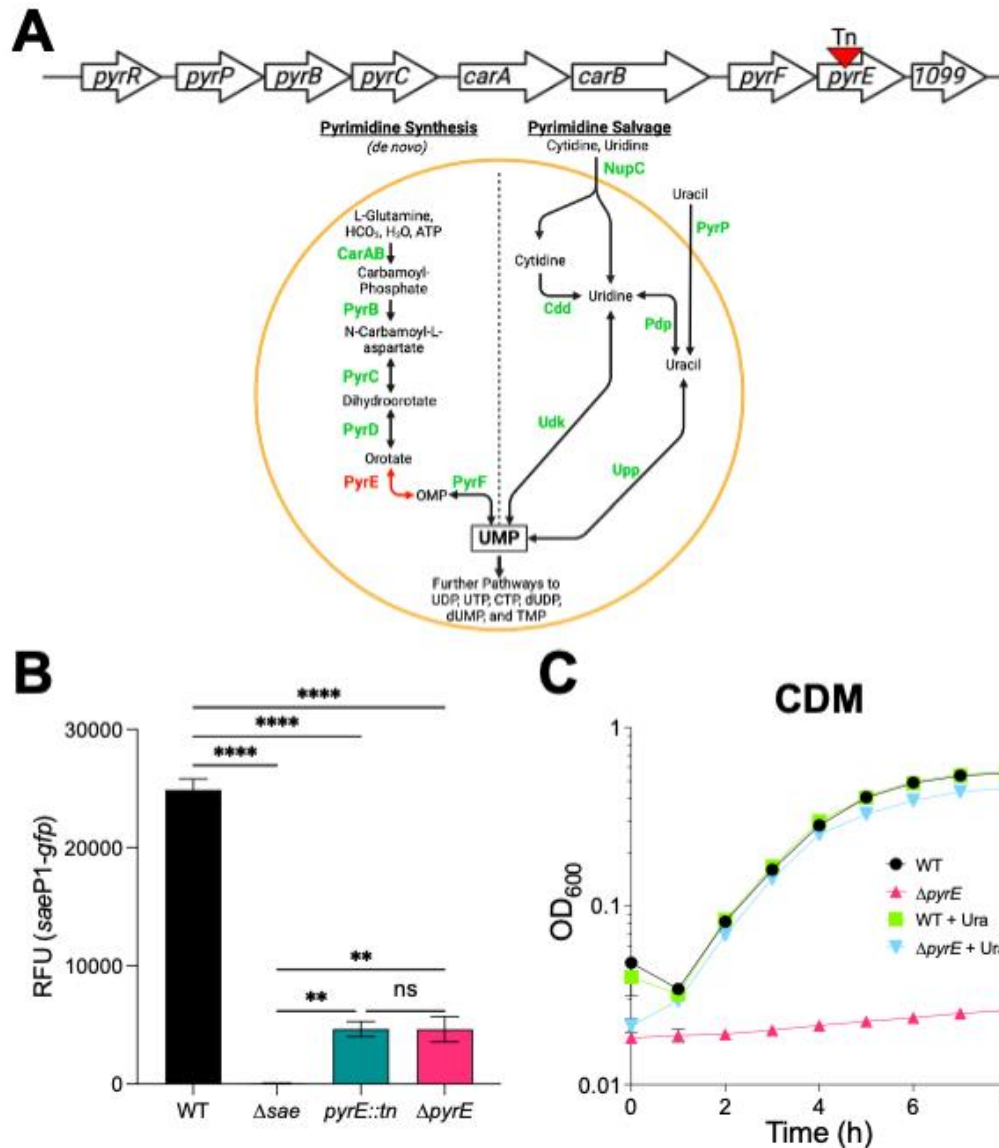
885   DiMaggio_Figure_1_V4.tiff

886   **Figure 1: Loss of *pyrE* results in lower basal *sae*P1 promoter activity and**

887   **pyrimidine auxotrophy. (A)** (Top) Pyrimidine biosynthetic gene cluster of *S. aureus*

888   annotated by homology to that of *Bacillus subtilis.* The transposon insertion identified in

889   *pyrE* is indicated with an inverted red triangle. (Bottom) Current understanding of *de*

890   *novo* and salvage pathways for pyrimidine biosynthesis in *S. aureus,* by analogy to the

45

891 model organism *B. subtilis.* PyrR bifunctional pyrimidine regulatory protein, uracil

892 phosphoribosyltransferase; CarAB, carbamoyl phosphate synthetase small and large

893 subunits; PyrB, aspartate carbamoyltransferase; PyrC, dihydroorotase; PyrD,

894 dihydroorotate dehydrogenase; PyrE orotate phosphoribosyltransferase; PyrF, orotidine

895 5'-phosphate decarboxylase; NupC, nucleotide permease; PyrP, uracil permease; Cdd,

896 cytidine deaminase; Pdp, pyrimidine nucleoside phosphorylase; Udk, uridine kinase;

897 Upp, uracil phosphoribosyltransferase (12, 14, 98) **(B)** The indicated LAC strains were

898 grown in TSB to stationary phase (16 h), at which time *sae*P1 promoter activity was

899 measured. Data are plotted as relative fluorescent units (RFU [GFP/OD$_{600}$]). **(C)** Wild

900 type (WT) and Δ*pyrE* mutant strains were grown in chemically defined medium (CDM) ±

901 uracil supplementation (Ura; 200 µM). Growth was monitored as increase in absorbance

902 at 600 nm (OD$_{600}$) and plotted over time. For panels B and C, data are representative of

903 at least three independent experiments and plotted as mean ± SEM. For panel C, error

904 bars are plotted for all time points; in many cases they are too small to be seen.

905 ****p<0.0001 relative to WT, One-way ANOVA with Tukey's post-test. ns, not significant.

906
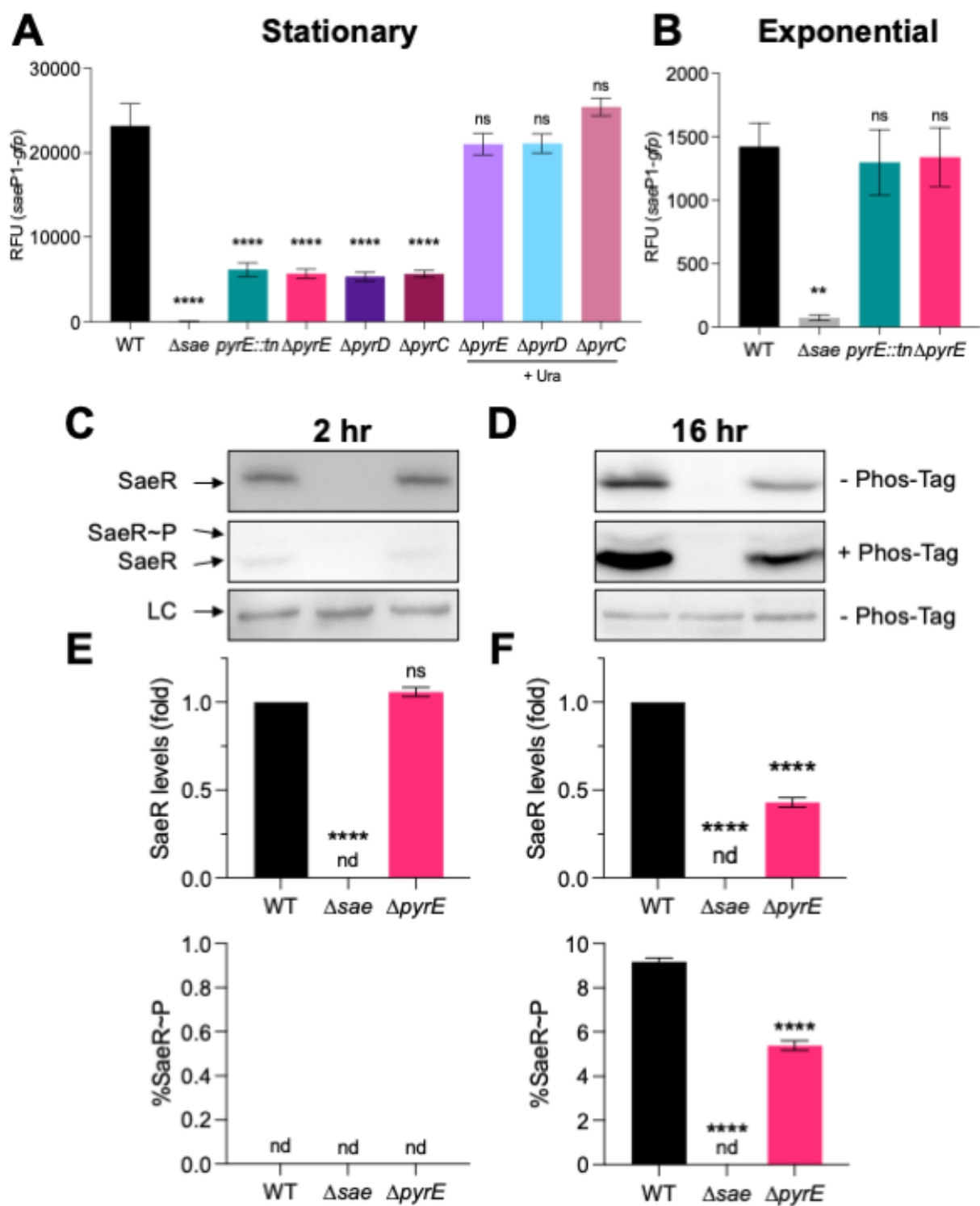
907

908   DiMaggio_Figure_2_V4.tiff

909   **Figure 2: Pyrimidine limitation reduces SaeS kinase activity.** The indicated strains

910   carrying the *sae*P1-*gfp* reporter were grown in TSB ± uracil supplementation (Ura; 200

911   µM) to **(A)** stationary phase (16 h) and **(B)** exponential phase (2 h), at which time *sae*P1

912   promoter activity was measured. **(C-H)** Measurement of intracellular SaeR species. The

913   indicated strains were grown in TSB to exponential phase (2 h) and stationary phases

914   (16 h), at which times cell pellets were collected, normalized by OD_{600}, and cell lysates

915   then subjected to Western Blot analysis. **(C and D)** Representative Western blots (top

916   and bottom) and Phos-tag Western blots (middle) of cell lysates using antibodies

917   recognizing SaeR. **(E and F)** Analysis of SaeR species using Multi Gauge software

918   (FujiFilm) showing SaeR levels relative to WT in each condition (Top), and the

919   percentage of SaeR~P relative to the total amount of SaeR in each sample (bottom). All

920   data are from at least three independent experiments and are plotted as mean ± SEM.

921   ****$p<0.0001$, **$p<0.01$,*$p<0.05$; One-way ANOVA with Dunnet's post-test relative to

922   respective WT. LC, loading control; nd, below detectible limit; ns, not significant.

923

48
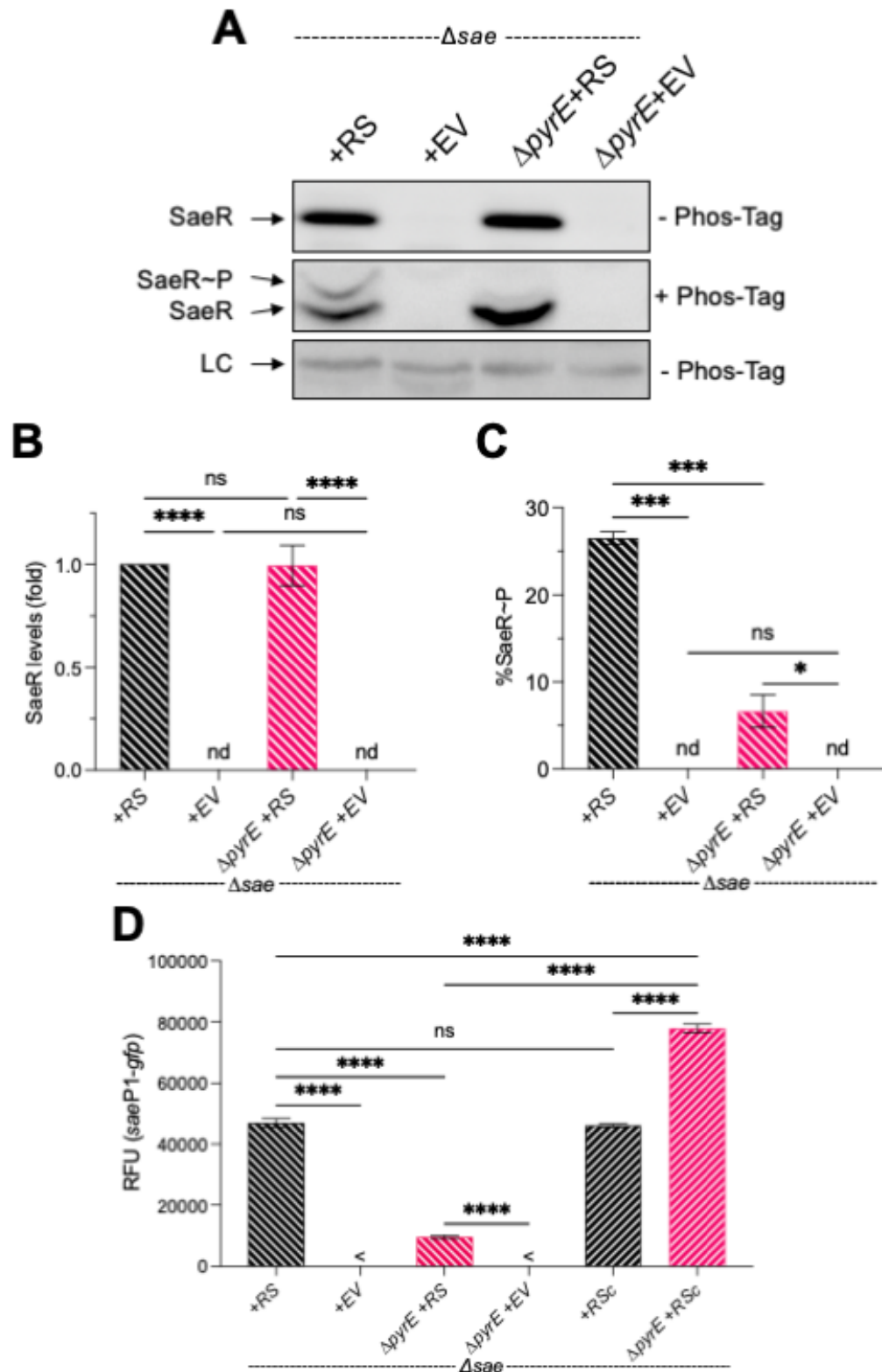
924

925   DiMaggio_Figure_3_V5.tiff

49

926 **Figure 3: The effect of pyrimidine limitation is independent of autoregulation and**

927 **acts at the membrane (A-C)** SaeR species present in SaePQRS-deficient strains

928 (Δ*sae*) with either *saeRS* complemented back under control of the constitutive P3

929 promoter (+RS) or the empty vector (+EV) grown in TSB to stationary phase (16 h). Cell

930 pellets were collected, normalized by OD_{600}, and lysates subsequently subjected to

931 Western Blot analysis using polyacrylamide gels ± Phos-tag acrylamide. **(A)**

932 Representative blots are shown. **(B and C)** Densitometry analysis was performed,

933 quantifying levels of the different SaeR species present in each sample. LC, loading

934 control; nd, below detectible limit. **(D)** Measurement of *sae*P1-*gfp* promoter activity in

935 stationary phase cultures (16 h) with either empty vector (EV), full length SaeS (+*RS*),

936 or the cytosolic, catalytic domain of SaeS (+*RSc*). <, fluorescence was undetectable

937 relative to blank containing PBS. For all panels, data are plotted as mean ± SEM, n≥3.

938 ****p<0.0001, ***p<0.001, *p<0.05, one-way ANOVA with Tukey's post-test. ns, not

939 significant.

940

941   DiMaggio_Figure_4_V4.tiff
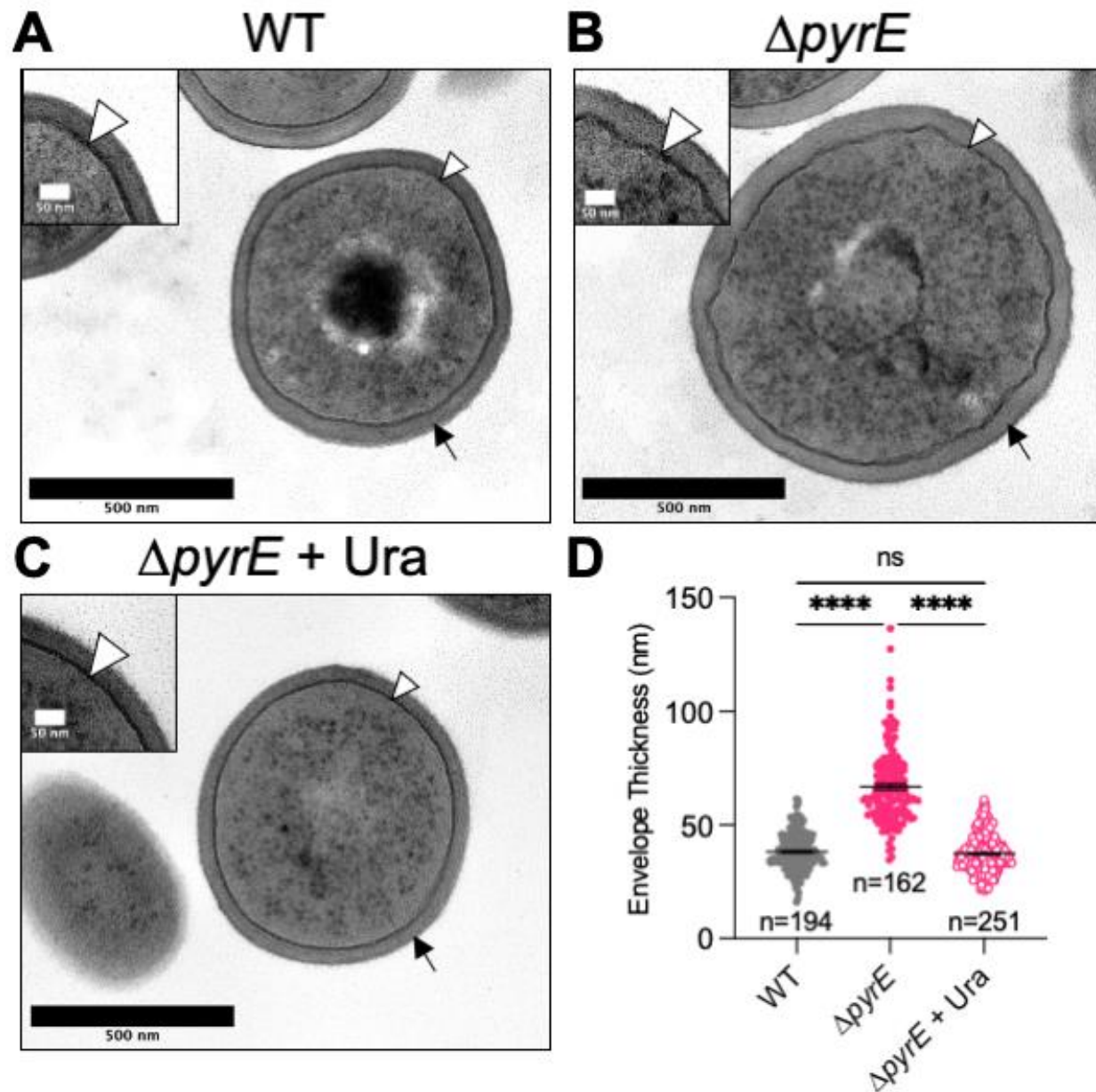
942   **Figure 4: Δ*pyrE* mutant cells have a thickened cell wall and a crenulated**

943   **membrane.** Representative TEM images of the **(A)** wild-type (WT), **(B)** Δ*pyrE* mutant,

944   and **(C)** Δ*pyrE* mutant chemically complemented with uracil (Ura; 200 μM). Inset images

945   emphasize the crenulated cell membrane architecture of the Δ*pyrE* mutant. **(D)**

946   Measurements of cell envelope thickness from cell membrane to cell wall edge were

947   performed in FIJI as described in *Materials and Methods* with one measurement per

948   individual cell indicated below the dot plot. Data are plotted as mean ± SEM from three

949   biological replicates, with bars indicating the mean thickness and error bars indicating

950   SEM. White arrowheads point to the membrane; black arrowheads point to cell wall,

951   ****$p<0.0001$; ns, not significant; one-way ANOVA with Tukey's post-test.
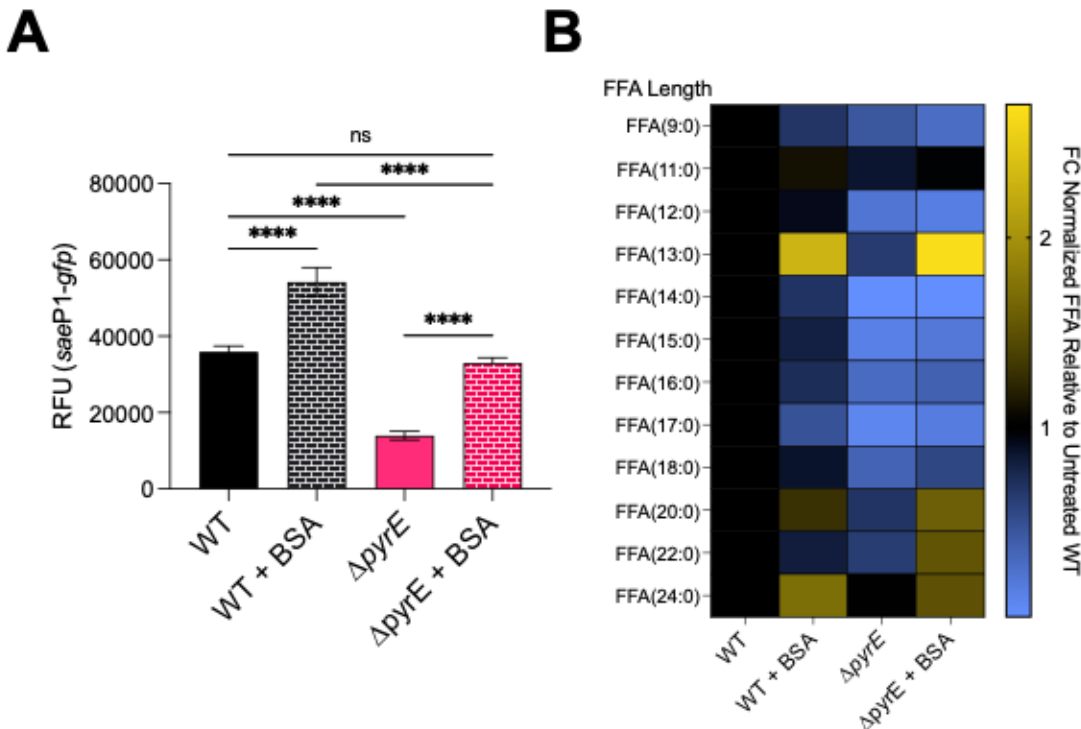
DiMaggio_Figure_5_V5.tiff

Figure 5: Treatment with bovine serum albumin restores Sae activity and promotes release of free fatty acids during pyrimidine limitation. (A) The indicated strains carrying the *sae*P1-*gfp* reporter were grown in TSB ± BSA (10 mg/mL^{-1}) to stationary phase, at which time *sae*P1 promoter activity was measured. Data are plotted as mean ± SEM. (B) Culture supernatants from the indicated strains were collected, FFAs were extracted, and extracts were subjected to LC-MS/MS analysis. Data were normalized using an internal standard (d4-Palmitic acid) and mean fold change (FC) in abundances of free fatty acids (FFA) relative to WT are depicted using a heat map. All data are from at least three biological replicates ****p<0.0001; ns, not significant; One-way ANOVA with Tukey's post-test.
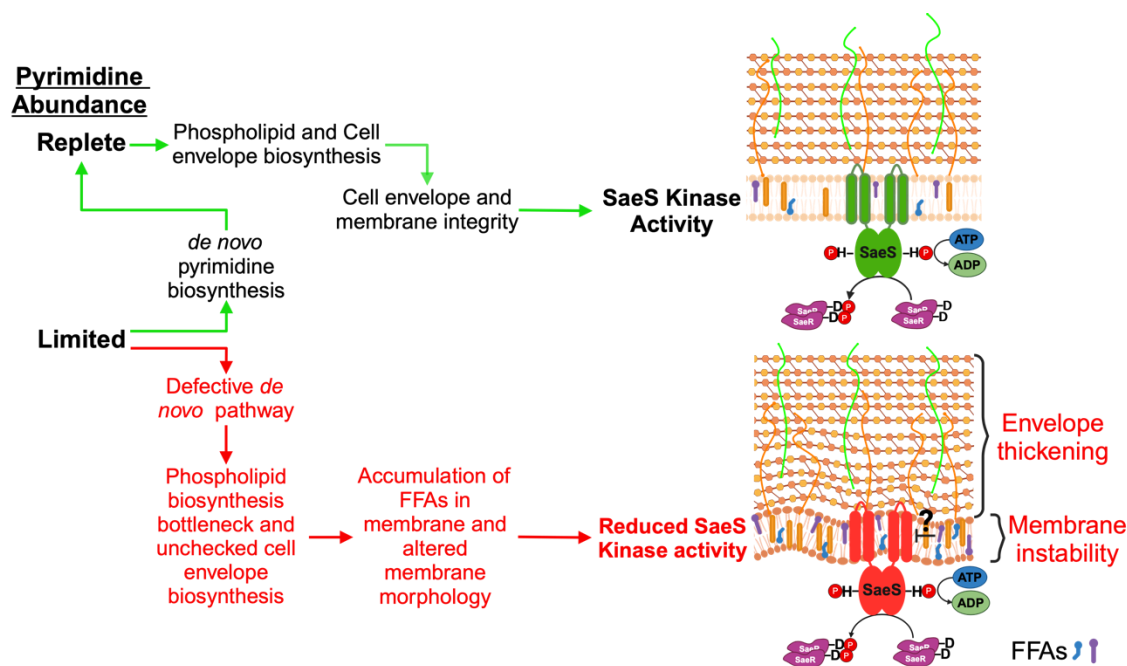
DiMaggio_Figure_6.PDF

Figure 6: Working model for proposed mechanism by which pyrimidines promote SaeS kinase activity. During cellular growth, pyrimidine sufficiency dictates whether *S. aureus* needs to turn on the *de novo* pyrimidine biosynthetic pathway. Pyrimidines promote SaeS kinase activity, in part, by promoting and maintaining cell envelope and membrane integrity. Under pyrimidine-limited conditions where *S. aureus* cannot synthesize pyrimidines *de novo*, cell envelope biosynthesis goes unchecked, resulting in increased LTA production, thickening of the cell wall, and formation of a bottleneck in phospholipid biosynthesis. This results in an unstable membrane due to accumulation of phospholipid precursors, including free fatty acids, that act to reduce SaeS kinase activity.

54

981
982   Bibliography and References Cited:
983
984   1.   Otto M. 2010. *Staphylococcus* colonization of the skin and antimicrobial peptides.
985   Expert Rev Dermatol 5:183-195.
986   2.   Wertheim HFL, Vos MC, Ott A, van Belkum A, Voss A, Kluytmans JAJW, van
987   Keulen PHJ, Vandenbroucke-Grauls CMJE, Meester MHM, Verbrugh HA. 2004.
988   Risk and outcome of nosocomial Staphylococcus aureus bacteraemia in nasal
989   carriers versus non-carriers. The Lancet 364:703-705.
990   3.   Wertheim HF, Melles DC, Vos MC, van Leeuwen W, van Belkum A, Verbrugh HA,
991   Nouwen JL. 2005. The role of nasal carriage in Staphylococcus aureus
992   infections. Lancet Infect Dis 5:751-62.
993   4.   Kluytmans JAJW, Wertheim HFL. 2005. Nasal Carriage of Staphylococcus
994   aureus and Prevention of Nosocomial Infections. Infection 33:3-8.
995   5.   Lowy F. 1998. *Staphylococcus aureus* infections. N Engl J Med 339:520-532.
996   6.   Vandenesch F, Naimi T, Enright M, Lina G, Nimmo G, Heffernan H, Liassine N,
997   Bes M, Greenland T, Reverdy M, Etienne J. 2003. Community-acquired
998   methicillin-resistant *Staphylococcus aureus* carrying Panton-Valentine leukocidin
999   genes: worldwide emergence. Emerg Infect Dis 9:978-984.
1000 7.   Fowler VG, Jr., Miro JM, Hoen B, Cabell CH, Abrutyn E, Rubinstein E, Corey GR,
1001   Spelman D, Bradley SF, Barsic B, Pappas PA, Anstrom KJ, Wray D, Fortes CQ,
1002   Anguera I, Athan E, Jones P, van der Meer JT, Elliott TS, Levine DP, Bayer AS.
1003   2005. Staphylococcus aureus endocarditis: a consequence of medical progress.
1004   Jama 293:3012-21.
1005 8.   Berendt T, Byren I. 2004. Bone and joint infection. Clin Med (Lond) 4:510-8.
1006 9.   Copin R, Sause WE, Fulmer Y, Balasubramanian D, Dyzenhaus S, Ahmed JM,
1007   Kumar K, Lees J, Stachel A, Fisher JC, Drlica K, Phillips M, Weiser JN, Planet
1008   PJ, Uhlemann AC, Altman DR, Sebra R, van Bakel H, Lighter J, Torres VJ,
1009   Shopsin B. 2019. Sequential evolution of virulence and resistance during clonal
1010   spread of community-acquired methicillin-resistant Staphylococcus aureus. Proc
1011   Natl Acad Sci U S A 116:1745-1754.
1012 10. Lee B, Singh A, David M, Bartsch S, Slayton R, Huang S, Zimmer S, Potter M,
1013   Macal C, Lauderdale D, Miller L, Daum R. 2013. The economic burden of
1014   community-associated methicillin-resistant *Staphylococcus aureus* (CA-MRSA).
1015   Clin Microbiol Infect 19:528-536.
1016 11. Kriegeskorte A, Block D, Drescher M, Windmüller N, Mellmann A, Baum C,
1017   Neumann C, Lorè Nicola I, Bragonzi A, Liebau E, Hertel P, Seggewiss J, Becker
1018   K, Proctor Richard A, Peters G, Kahl Barbara C. 2014. Inactivation of thyA in
1019   Staphylococcus aureus Attenuates Virulence and Has a Strong Impact on
1020   Metabolism and Virulence Gene Expression. mBio 5:10.1128/mbio.01447-14.
1021 12. Switzer RL, Zalkin H, Saxild HH. 2002. Purine, pyrimidine, and pyridine
1022   nucleotide metabolism, p 255-269. *In* Sonenshein AL, Hoch JA, Losick R (ed),
1023   *Bacillus subtilis* and its closest relatives: from genes to cells. ASM Press,
1024   Washington, D.C.
1025 13. Goncheva MI, Chin D, Heinrichs DE. 2022. Nucleotide biosynthesis: the base of
1026   bacterial pathogenesis. Trends in Microbiology 30:793-804.

1027   14.   Potvin BW, Kelleher RJ, Jr., Gooder H. 1975. Pyrimidine biosynthetic pathway of
1028   Baccillus subtilis. J Bacteriol 123:604-15.
1029   15.   Niazy A, Hughes LE. 2015. Accumulation of Pyrimidine Intermediate Orotate
1030   Decreases Virulence Factor Production in Pseudomonas aeruginosa. Curr
1031   Microbiol 71:229-34.
1032   16.   Yang H-J, Bogomolnaya L, McClelland M, Andrews-Polymenis H. 2017. De novo
1033   pyrimidine synthesis is necessary for intestinal colonization of Salmonella
1034   Typhimurium in chicks. PLOS ONE 12:e0183751.
1035   17.   Turner RJ, Lu Y, Switzer RL. 1994. Regulation of the Bacillus subtilis pyrimidine
1036   biosynthetic (pyr) gene cluster by an autogenous transcriptional attenuation
1037   mechanism. Journal of Bacteriology 176:3708-3722.
1038   18.   Fields CJ, Switzer RL. 2007. Regulation of pyr Gene Expression in
1039   Mycobacterium smegmatis by PyrR-Dependent Translational Repression.
1040   Journal of Bacteriology 189:6236-6245.
1041   19.   Tomchick DR, Turner RJ, Switzer RL, Smith JL. 1998. Adaptation of an enzyme
1042   to regulatory function: structure of the *Bacillus subtilis* PyrR, a *pyr* RNA-binding
1043   attenuation protein and uracil phosphoribosyltransferase. Structure 6.
1044   20.   Turner RJ, Bonner ER, Grabner GK, Switzer RL. 1998. Purification and
1045   characterization of *Bacillus subtilis* PyrR, a bifunctional *pyr* mRNA-binding
1046   attenuation protein/uracil phosphoribosyltransferase. J Biol Chem 273:5932-
1047   5938.
1048   21.   Valentino M, Foulston L, Sadaka A, Kos V, Villet R, Santa Maria JJ, Lazinski D,
1049   Camilli A, Walker S, Hooper D, Gilmore M. 2014. Genes contributing to
1050   *Staphylococcus aureus* fitness in abscess- and infection-related ecologies. MBio
1051   5:e01729-14.
1052   22.   West SA, Griffin AS, Gardner A, Diggle SP. 2006. Social evolution theory for
1053   microorganisms. Nature Reviews Microbiology 4:597-607.
1054   23.   Davis KM. 2020. For the Greater (Bacterial) Good: Heterogeneous Expression of
1055   Energetically Costly Virulence Factors. Infect Immun 88.
1056   24.   Somerville GA, Saïd-Salim B, Wickman JM, Raffel SJ, Kreiswirth BN, Musser JM.
1057   2003. Correlation of acetate catabolism and growth yield in Staphylococcus
1058   aureus: implications for host-pathogen interactions. Infect Immun 71:4724-32.
1059   25.   Dufresne K, DiMaggio DAJ, Maduta CS, Brinsmade SR, McCormick JK. 2024.
1060   Discovery of an antivirulence compound that targets the *Staphylococcus aureus*
1061   SaeRS two-component system to inhibit toxic shock syndrome toxin-1
1062   production. J Biol Chem 300:107455.
1063   26.   Dehbanipour R, Ghalavand Z. 2022. Anti-virulence therapeutic strategies against
1064   bacterial infections: recent advances. Germs 12:262-275.
1065   27.   Dickey SW, Cheung GYC, Otto M. 2017. Different drugs for bad bugs:
1066   antivirulence strategies in the age of antibiotic resistance. Nat Rev Drug Discov
1067   16:457-471.
1068   28.   Liu Q, Yeo WS, Bae T. 2016. The SaeRS Two-Component System of
1069   *Staphylococcus aureus*. Genes (Basel) 7:E81.
1070   29.   Giraudo A, Calzolari A, Cataldi A, Bogni C, Nagel R. 1999. The *sae* locus of
1071   *Staphylococcus aureus* encodes a two-component regulatory system. FEMS
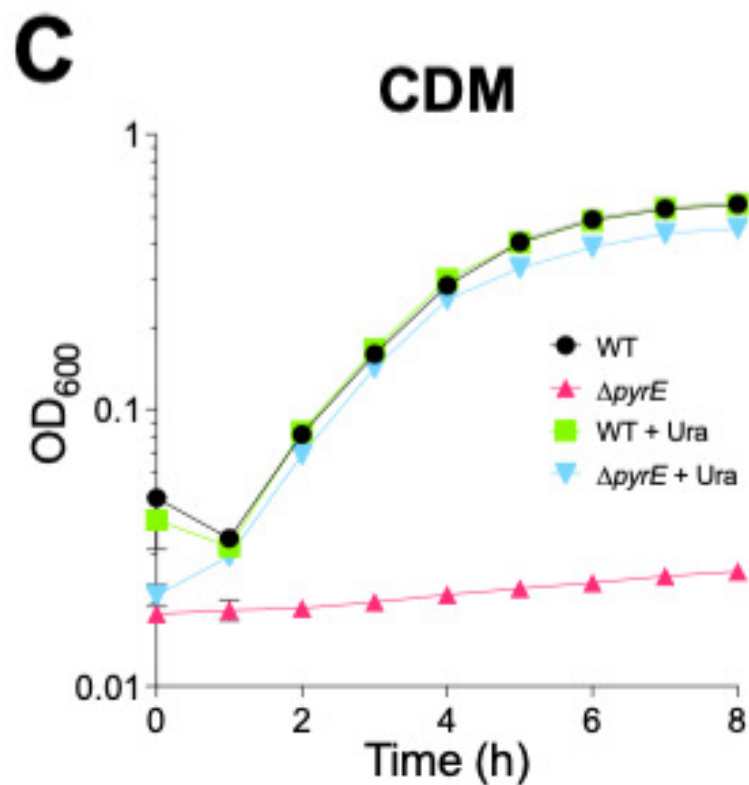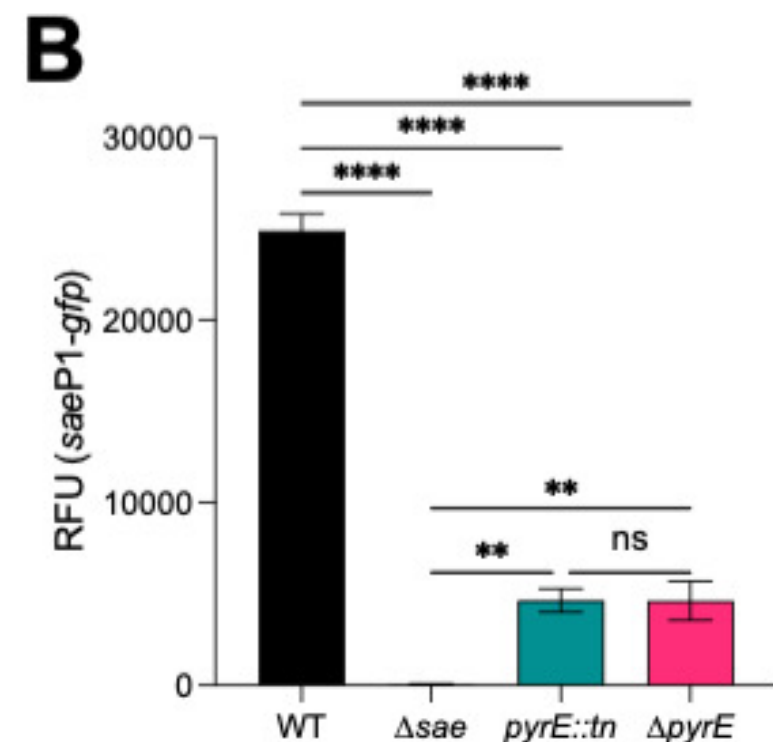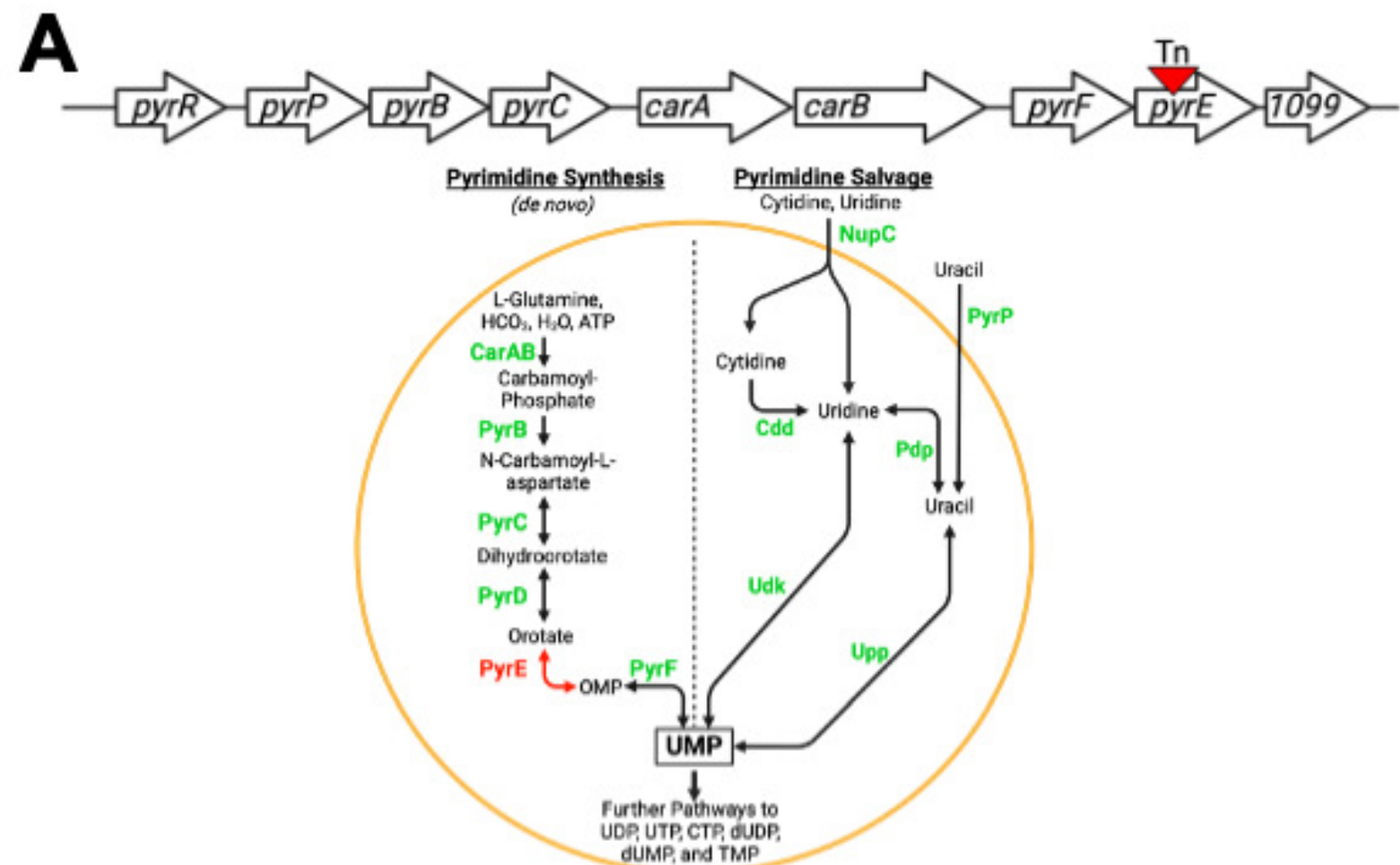1072   Microbiol Lett 177:15-22.

30. Giraudo AT, Cheung AL, Nagel R. 1997. The *sae* locus of *Staphylococcus aureus* controls exoprotein synthesis at the transcriptional level. Arch Microbiol 168:53-58.

31. Giraudo AT, Mansilla C, Chan A, Raspanti C, Nagel R. 2003. Studies on the expression of regulatory locus *sae* in *Staphylococcus aureus*. Curr Microbiol 46:246-250.

32. Giraudo AT, Raspanti CG, Calzolari A, Nagel R. 1994. Characterization of a Tn551-mutant of *Staphylococcus aureus* defective in the production of several exoproteins. Can J Microbiol 40:677-681.

33. Jeong DW, Cho H, Jones MB, Shatzkes K, Sun F, Ji Q, Liu Q, Peterson SN, He C, Bae T. 2012. The auxiliary protein complex SaePQ activates the phosphatase activity of sensor kinase SaeS in the SaeRS two-component system of *Staphylococcus aureus*. Mol Microbiol 86:331-348.

34. Jeong DW, Cho H, Lee H, Li C, Garza J, Fried M, Bae T. 2011. Identification of the P3 promoter and distinct roles of the two promoters of the SaeRS two-component system in *Staphylococcus aureus*. J Bacteriol 193:4672-4684.

35. Geiger T, Goerke C, Mainiero M, Kraus D, Wolz C. 2008. The virulence regulator Sae of *Staphylococcus aureus*: promoter activities and response to phagocytosis-related signals. J Bacteriol 190:3419-3428.

36. Gao R, Stock AM. 2009. Biological insights from structures of two-component proteins. Annu Rev Microbiol 63:133-54.

37. Bhate MP, Molnar KS, Goulian M, DeGrado WF. 2015. Signal transduction in histidine kinases: insights from new structures. Structure 23:981-94.

38. Cho H, Jeong DW, Li C, Bae T. 2012. Organizational requirements of the SaeR binding sites for a functional P1 promoter of the *sae* operon in *Staphylococcus aureus*. J Bacteriol 194:2865-2876.

39. Sun F, Li C, Jeong D, Sohn C, He C, Bae T. 2010. In the Staphylococcus aureus two-component system sae, the response regulator SaeR binds to a direct repeat sequence and DNA binding requires phosphorylation by the sensor kinase SaeS. J Bacteriol 192:2111-27.

40. Liu Q, Cho H, Yeo WS, Bae T. 2015. The extracytoplasmic linker peptide of the sensor protein SaeS tunes the kinase activity required for staphylococcal virulence in response to host signals. PLoS Pathog 11:e1004799.

41. Mascher T. 2006. Intramembrane-sensing histidine kinases: a new family of cell envelope stress sensors in Firmicutes bacteria. FEMS Microbiology Letters 264:133-144.

42. Mlynek KD, Sause WE, Moormeier DE, Sadykov MR, Hill KR, Torres VJ, Bayles KW, Brinsmade SR. 2018. Nutritional regulation of the Sae two-component system by CodY in Staphylococcus aureus. J Bacteriol 200:e00012-18.

43. Alqahtani S, DiMaggio Jr DA, Brinsmade SR. 2024. CodY controls the SaeR/S two-component system by modulating branched-chain fatty acid synthesis in *Staphylococcus aureus*. J Bacteriol In press.

44. Pendleton A, Yeo WS, Alqahtani S, DiMaggio Jr DA, Stone CJ, Li Z, Singh VK, Montgomery CP, Bae T, Brinsmade SR. 2022. Regulation of the Sae Two-Component System by Branched-Chain Fatty Acids in *Staphylococcus aureus*. mBio 13:e0147222.
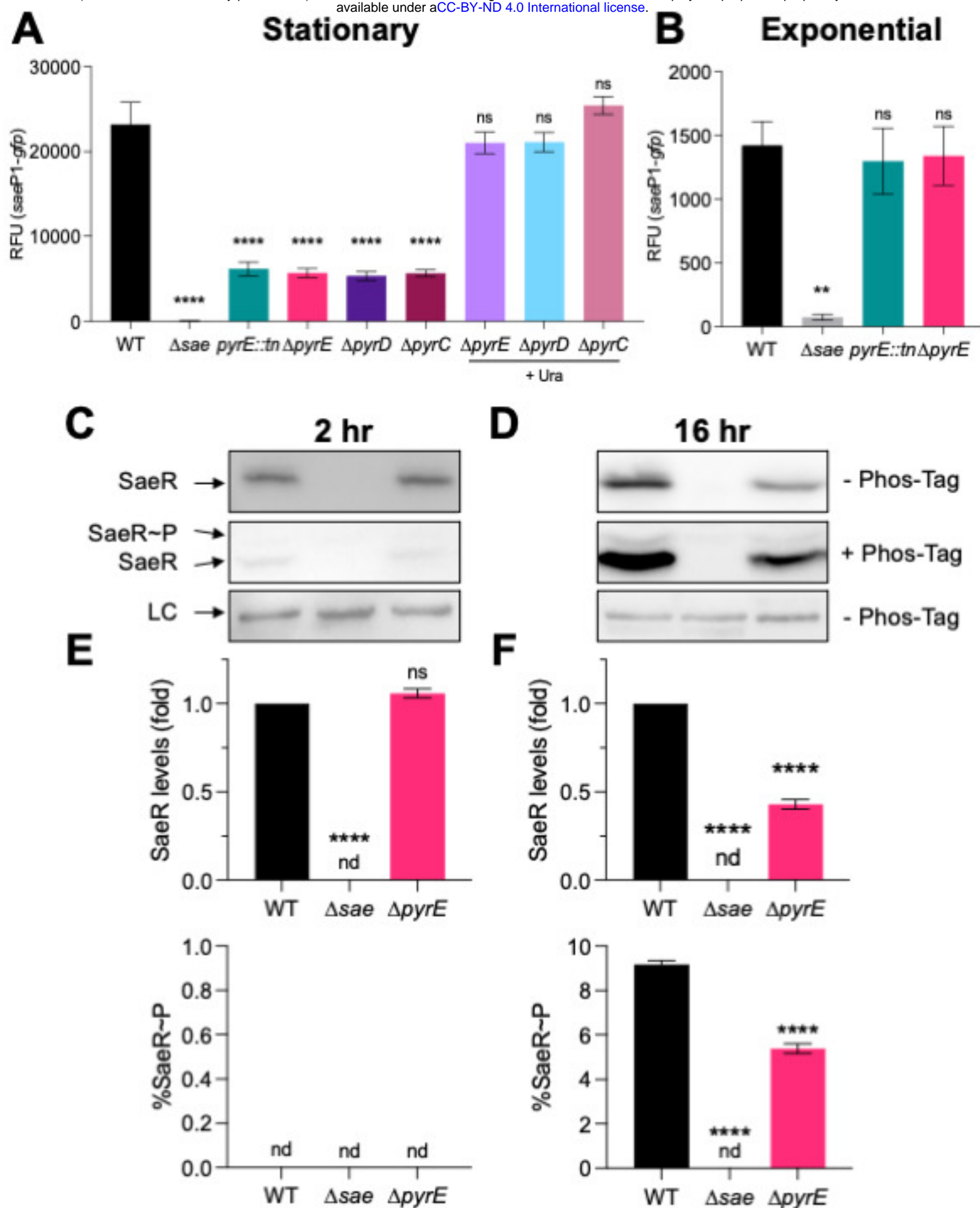
45. Zhao N, Wang Y, Liu J, Yang Z, Jian Y, Wang H, Ahmed M, Li M, Bae T, Liu Q. 2022. Molybdopterin biosynthesis pathway contributes to the regulation of SaeRS two-component system by ClpP in Staphylococcus aureus. Virulence 13:727-739.

46. Neuhard J, Nygaard P. 1987. Purines and Pyrimidines, p 445-473. *In* Neidhardt FC, Ingraham JL, Low KB, Magasanik B, Schaechter M, Umbarger HE (ed), *Escherichia coli* and *Salmonella typhimurium:* Cellular and Molecular Biology, vol 1. American Society for Microbiology, Washington, D.C.

47. Charlier D, Nguyen Le Minh P, Roovers M. 2018. Regulation of carbamoylphosphate synthesis in Escherichia coli: an amazing metabolite at the crossroad of arginine and pyrimidine biosynthesis. Amino Acids 50:1647-1661.

48. Villanueva M, Garcia B, Valle J, Rapun B, Ruiz de Los Mozos I, Solano C, Marti M, Penades JR, Toledo-Arana A, Lasa I. 2018. Sensory deprivation in Staphylococcus aureus. Nat Commun 9:523.

49. Barbieri CM, Stock AM. 2008. Universally applicable methods for monitoring response regulator aspartate phosphorylation both in vitro and in vivo using Phos-tag-based reagents. Anal Biochem 376:73-82.

50. Novick R, Jiang D. 2003. The staphylococcal *saeRS* system coordinates environmental signals with *agr* quorum sensing. Microbiology 149:2709-2717.

51. Steinhuber A, Goerke C, Bayer MG, Döring G, Wolz C. 2003. Molecular architecture of the regulatory Locus sae of *Staphylococcus aureus* and its impact on expression of virulence factors. J Bacteriol 185:6278-6286.

52. Rudra P, Boyd JM. 2020. Metabolic control of virulence factor production in Staphylococcus aureus. Current Opinion in Microbiology 55:81-87.

53. Kanehisa M, Goto S. 2000. KEGG: kyoto encyclopedia of genes and genomes. Nucleic Acids Res 28:27-30.

54. Tenenbaum D. 2016. KEGGREST: Client-side REST access to KEGG. R package version 1.

55. Kanehisa M, Furumichi M, Tanabe M, Sato Y, Morishima K. 2017. KEGG: new perspectives on genomes, pathways, diseases and drugs. Nucleic Acids Res 45:D353-d361.

56. Bleul L, Francois P, Wolz C. 2021. Two-Component Systems of S. aureus: Signaling and Sensing Mechanisms. Genes (Basel) 13.

57. Groisman EA. 2016. Feedback Control of Two-Component Regulatory Systems. Annu Rev Microbiol 70:103-24.

58. Wang B, Zhao A, Novick Richard P, Muir Tom W. 2014. Activation and Inhibition of the Receptor Histidine Kinase AgrC Occurs through Opposite Helical Transduction Motions. Molecular Cell 53:929-940.

59. CLSI. 2018. Methods for dilution antimicrobial susceptibility tests for bacteria that grow aerobically, p 27-50, CLSI standard M07-A11, 11 ed.

60. Lee JH. 2003. Methicillin (Oxacillin)-resistant Staphylococcus aureus strains isolated from major food animals and their potential transmission to humans. Appl Environ Microbiol 69:6489-94.

61. Zeden MS, Gallagher LA, Bueno E, Nolan AC, Ahn J, Shinde D, Razvi F, Sladek M, Burke Ó, O'Neill E, Fey PD, Cava F, Thomas VC, O'Gara JP. 2023. Metabolic reprogramming and altered cell envelope characteristics in a pentose phosphate

pathway mutant increases MRSA resistance to β-lactam antibiotics. PLOS Pathogens 19:e1011536.

62. Falagas Matthew E, Vouloumanou Evridiki K, Samonis G, Vardakas Konstantinos Z. 2020. Fosfomycin. Clinical Microbiology Reviews 29:321-347.

63. Vickery CR, Wood BM, Morris HG, Losick R, Walker S. 2018. Reconstitution of Staphylococcus aureus Lipoteichoic Acid Synthase Activity Identifies Congo Red as a Selective Inhibitor. Journal of the American Chemical Society 140:876-879.

64. Bonini D, Duggan S, Alnahari A, Brignoli T, Strahl H, Massey RC. 2024. Lipoteichoic acid biosynthesis by Staphylococcus aureus is controlled by the MspA protein. mBio 15:e0151224.

65. Duggan S, Laabei M, Alnahari AA, O'Brien EC, Lacey KA, Bacon L, Heesom K, Fu CL, Otto M, Skaar E, McLoughlin RM, Massey RC. 2020. A Small Membrane Stabilizing Protein Critical to the Pathogenicity of Staphylococcus aureus. Infect Immun 88.

66. Múnera-Jaramillo J, López G-D, Suesca E, Carazzone C, Leidy C, Manrique-Moreno M. 2024. The role of staphyloxanthin in the regulation of membrane biophysical properties in Staphylococcus aureus. Biochimica et Biophysica Acta (BBA) - Biomembranes 1866:184288.

67. Mishra NN, Liu GY, Yeaman MR, Nast CC, Proctor RA, McKinnell J, Bayer AS. 2011. Carotenoid-related alteration of cell membrane fluidity impacts Staphylococcus aureus susceptibility to host defense peptides. Antimicrob Agents Chemother 55:526-31.

68. Kennedy EP. 1956. The synthesis of cytidine diphosphate choline, cytidine diphosphate ethanolamine, and related compounds. J Biol Chem 222:185-191.

69. Blunsom NJ, Cockcroft S. 2020. CDP-Diacylglycerol Synthases (CDS): Gateway to Phosphatidylinositol and Cardiolipin Synthesis. Front Cell Dev Biol 8:63.

70. Kuhn S, Slavetinsky CJ, Peschel A. 2015. Synthesis and function of phospholipids in Staphylococcus aureus. International Journal of Medical Microbiology 305:196-202.

71. Ericson ME, Subramanian C, Frank MW, Rock CO. 2017. Role of Fatty Acid Kinase in Cellular Lipid Homeostasis and SaeRS-Dependent Virulence Factor Expression in Staphylococcus aureus. mBio 8.

72. DeMars ZR, Krute CN, Ridder MJ, Gilchrist AK, Menjivar C, Bose JL. 2021. Fatty acids can inhibit Staphylococcus aureus SaeS activity at the membrane independent of alterations in respiration. Mol Microbiol 116:1378-1391.

73. Goto K, Mizushima S. 1978. Removal by bovine serum albumin of fatty acids from membrane vesicles and its effect on proline transport activity in Escherichia coli. J Biochem 84:251-8.

74. Ferreira MCdS, Pendleton A, Yeo WS, Málaga Gadea FC, Camelo D, McGuire M, Brinsmade SR. 2024. In *Staphylococcus aureus*, the acyl-CoA synthetase MbcS supports branched-chain fatty acid synthesis from carboxylic acid and aldehyde precursors. Mol Microbiol 121:865-881.

75. Connolly J, Boldock E, Prince LR, Renshaw SA, Whyte MK, Foster SJ. 2017. Identification of Staphylococcus aureus Factors Required for Pathogenicity and Growth in Human Blood. Infect Immun 85.
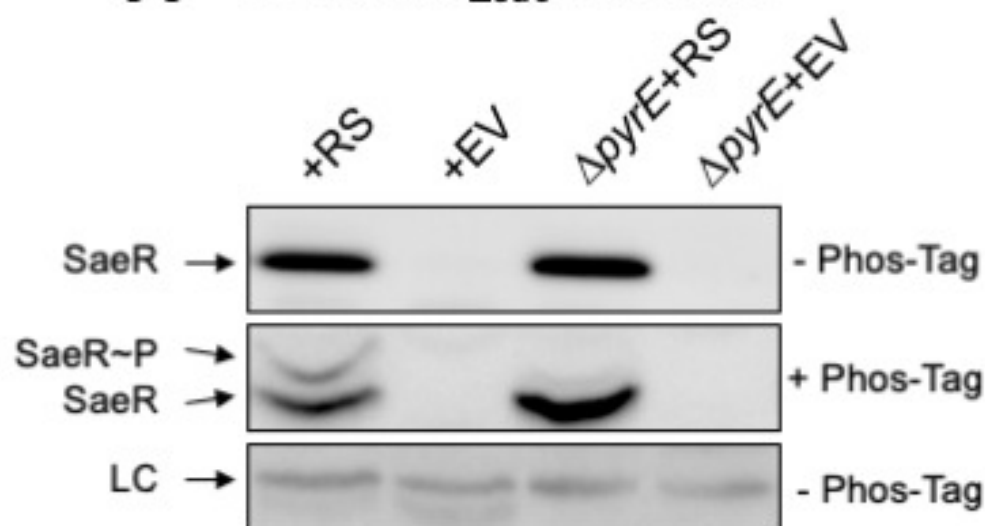
76. Sause WE, Balasubramanian D, Irnov I, Copin R, Sullivan MJ, Sommerfield A, Chan R, Dhabaria A, Askenazi M, Ueberheide B, Shopsin B, van Bakel H, Torres VJ. 2019. The purine biosynthesis regulator PurR moonlights as a virulence regulator in Staphylococcus aureus. Proceedings of the National Academy of Sciences 116:13563-13572.

77. King AN, Borkar SA, Samuels DJ, Batz Z, Bulock LL, Sadykov MR, Bayles KW, Brinsmade SR. 2018. Guanine limitation results in CodY-dependent and -independent alteration of *Staphylococcus aureus* physiology and gene expression. J Bacteriol 200:e00136-18.

78. Goncheva MI, Flannagan RS, Heinrichs DE. 2020. De Novo Purine Biosynthesis Is Required for Intracellular Growth of Staphylococcus aureus and for the Hypervirulence Phenotype of a purR Mutant. Infection and Immunity 88:10.1128/iai.00104-20.

79. Toh EA, Ohkusu M, Shimizu K, Takahashi-Nakaguchi A, Kawamoto S, Ishiwada N, Watanabe A, Kamei K. 2017. Putative orotate transporter of Cryptococcus neoformans, Oat1, is a member of the NCS1/PRT transporter super family and its loss causes attenuation of virulence. Curr Genet 63:697-707.

80. Burns VW. 1966. Regulation of pyrimidine biosynthesis and its strong coupling to the purine system. Biophys J 6:787-800.

81. Yeo WS, Dyzenhaus S, Torres VJ, Brinsmade SR, Bae T. 2023. Regulation of Bacterial Two-Component Systems by Cardiolipin. Infect Immun 91:e0004623.

82. Gründling A, Schneewind O. 2007. Synthesis of glycerol phosphate lipoteichoic acid in Staphylococcus aureus. Proceedings of the National Academy of Sciences 104:8478-8483.

83. Fedtke I, Mader D, Kohler T, Moll H, Nicholson G, Biswas R, Henseler K, Götz F, Zähringer U, Peschel A. 2007. A Staphylococcus aureus ypfP mutant with strongly reduced lipoteichoic acid (LTA) content: LTA governs bacterial surface properties and autolysin activity. Molecular Microbiology 65:1078-1091.

84. Burtchett Troy A, Shook John C, Hesse Laura E, Delekta Philip C, Brzozowski Robert S, Nouri A, Calas Alexa J, Spanoudis Catherine M, Eswara Prahathees J, Hammer Neal D. 2023. Crucial Role for Lipoteichoic Acid Assembly in the Metabolic Versatility and Antibiotic Resistance of Staphylococcus aureus. Infection and Immunity 91:e00550-22.

85. Sheldon JR, Marolda CL, Heinrichs DE. 2014. TCA cycle activity in Staphylococcus aureus is essential for iron-regulated synthesis of staphyloferrin A, but not staphyloferrin B: the benefit of a second citrate synthase. Mol Microbiol 92:824-39.

86. Bertani G. 1951. Studies on lysogenesis. I. The mode of phage liberation by lysogenic *Escherichia coli*. J Bacteriol 62:293-300.

87. Gibson DG, Young L, Chuang RY, Venter JC, Hutchison CA, 3rd, Smith HO. 2009. Enzymatic assembly of DNA molecules up to several hundred kilobases. Nat Methods 6:343-5.

88. Gibson DG, Glass JI, Lartigue C, Noskov VN, Chuang R-Y, Algire MA, Benders GA, Montague MG, Ma L, Moodie MM, Merryman C, Vashee S, Krishnakumar R, Assad-Garcia N, Andrews-Pfannkoch C, Denisova EA, Young L, Qi Z-Q, Segall-Shapiro TH, Calvey CH, Parmar PP, Hutchison CA, Smith HO, Venter JC. 2010.

1256   Creation of a Bacterial Cell Controlled by a Chemically Synthesized Genome.
1257   Science 329:52-56.

1258 89. Schenk S, Laddaga RA. 1992. Improved method for electroporation of
1259   *Staphylococcus aureus*. FEMS Microbiol Lett 73:133-138.

1260 90. Novick RP. 1991. Genetic systems in staphylococci. Methods Enzymol 204.

1261 91. Bae T, Schneewind O. 2006. Allelic replacement in Staphylococcus aureus with
1262   inducible counter-selection. Plasmid 55:58-63.

1263 92. Bolger AM, Lohse M, Usadel B. 2014. Trimmomatic: a flexible trimmer for
1264   Illumina sequence data. Bioinformatics 30:2114-20.

1265 93. Tjaden B. 2015. De novo assembly of bacterial transcriptomes from RNA-seq
1266   data. Genome Biology 16:1.

1267 94. McClure R, Balasubramanian D, Sun Y, Bobrovskyy M, Sumby P, Genco CA,
1268   Vanderpool CK, Tjaden B. 2013. Computational analysis of bacterial RNA-Seq
1269   data. Nucleic Acids Research 41:e140-e140.

1270 95. Karinou E, Schuster Christopher F, Pazos M, Vollmer W, Gründling A. 2018.
1271   Inactivation of the Monofunctional Peptidoglycan Glycosyltransferase SgtB
1272   Allows Staphylococcus aureus To Survive in the Absence of Lipoteichoic Acid.
1273   Journal of Bacteriology 201:10.1128/jb.00574-18.

1274 96. Morikawa K, Maruyama A, Inose Y, Higashide M, Hayashi H, Ohta T. 2001.
1275   Overexpression of sigma factor, sigma(B), urges Staphylococcus aureus to
1276   thicken the cell wall and to resist beta-lactams. Biochem Biophys Res Commun
1277   288:385-9.

1278 97. Schindelin J, Arganda-Carreras I, Frise E, Kaynig V, Longair M, Pietzsch T,
1279   Preibisch S, Rueden C, Saalfeld S, Schmid B, Tinevez J-Y, White DJ, Hartenstein
1280   V, Eliceiri K, Tomancak P, Cardona A. 2012. Fiji: an open-source platform for
1281   biological-image analysis. Nature Methods 9:676-682.

1282 98. Zhu H, Yang S-M, Yuan Z-M, Ban R. 2015. Metabolic and genetic factors
1283   affecting the productivity of pyrimidine nucleoside in Bacillus subtilis. Microbial
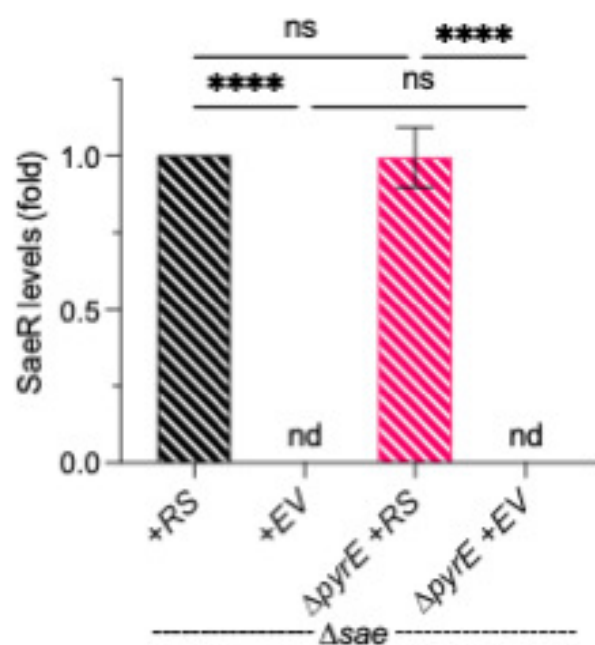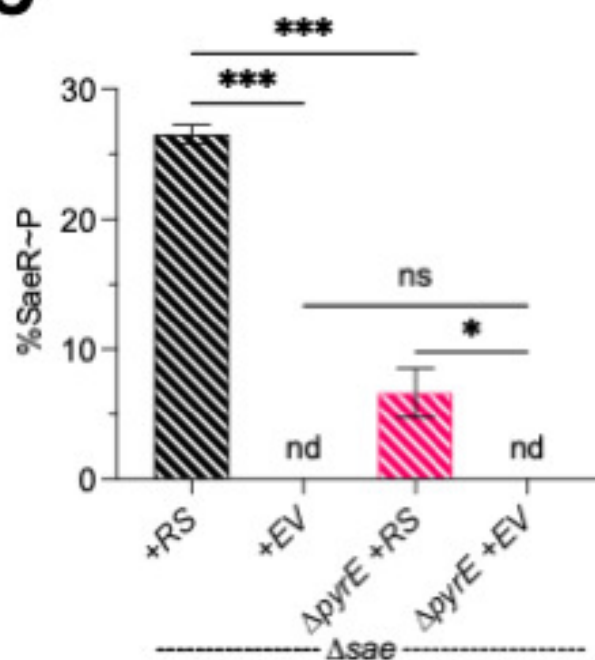1284   Cell Factories 14:54.

1285

1286

1287

1288

A

B